J. Fluid Mech. (2019), *vol.* 873, *pp.* 1179–1205.
doi:10.1017/jfm.2019.438

Linear interaction of two-dimensional free-stream disturbances with an oblique shock wave

Zhangfeng Huang[1,2,†,‡] **and Huilin Wang**[1]

[1]Department of Mechanics, Tianjin University, Tianjin 300072, PR China

[2]State Key Laboratory of Aerodynamics, China Aerodynamic Research and Development Center, Mianyang, Sichuan 621000, PR China

(Received 7 May 2018; revised 28 May 2019; accepted 28 May 2019; first published online 1 July 2019)

The problem of interaction between disturbances and shock waves was solved by a theoretical approach called linear interaction analysis in the mid-twentieth century. More recently, great progress has been made in analysing shock–turbulence interactions by direct numerical simulation. However, an unsolved theoretical problem remains: What happens when no acoustic waves are stimulated behind the shock wave? The concept of a damped wave is introduced, which is a type of excited plane wave. Based on this, the dispersion and amplitude relationships between any incident plane wave and resulting stimulated waves are constructed analytically, systematically and comprehensively. The physical essence of damped waves and the existence of critical angles are clarified. It is demonstrated that a damped wave is a complex number space solution to the acoustic dispersion relationship under certain conditions. It acts as a bridge connecting fast and slow acoustic waves at the position where the x component of the group velocity is zero. There are two critical angles that can excite fast and slow acoustic waves, which determine the conditions that stimulate a damped wave. Our results show good agreement with theoretical and simulation results. The contribution of each excited wave to the transmission coefficient is evaluated, the distribution of the transmission coefficient is analysed and application to an engineering wedge model is performed.

Key words: boundary layer receptivity, flow–structure interactions, shock waves

1. Introduction

The laminar–turbulent transition in supersonic and hypersonic boundary layers has received much attention in aerospace research. This transition is not only crucial in scientific research but also has importance in engineering applications, as it has economic implications (Arnal & Casalis 2000). The process of laminar–turbulent transition is complex and involves various components that depend on numerous parameters of the base flow and disturbances to it (Fedorov 2011). In supersonic and hypersonic aircraft in environments with weak turbulence, the transition mainly

† Email address for correspondence: hzf@tju.edu.cn

‡ The original version of this article was published with incorrect author information. A notice detailing this has been published and the error rectified in the online PDF and HTML copies.

involves a sequence of three stages (Zhong & Wang 2012): (1) receptivity, (2) linear eigenmode growth and (3) nonlinear breakdown to turbulence. The initial stage of transition, receptivity, refers to a process of converting external disturbances of the free stream into unstable waves in the boundary layers. It plays a key role in prediction of the laminar–turbulent transition, as it provides the initial amplitudes, frequencies and phases of the unstable waves in the boundary layers (Ma & Zhong 2003*a*,*b*, 2005).

During most supersonic/hypersonic flights, a shock wave is present near the head position of the vehicle. In this circumstance, research on receptivity focuses on two stages, in which (1) small perturbations in the free-stream interact with the shock wave and (2) various disturbances passing through the shock wave enter the boundary layer and excite unstable waves in it. Experimental results indicate that the mutual interaction of these small disturbances and the shock wave strongly affects the instability of boundary-layer flow and its transition characteristics (Potter & Whitfield 1962; Stetson *et al.* 1984).

There are two main approaches to studying interactions between disturbances and shock waves. One is a theoretical approach called linear interaction analysis (LIA) (Moore 1954; Ribner 1954), in which viscous and nonlinear effects are neglected across the shock wave and the interaction is treated analytically using linearized Euler equations and Rankine–Hugoniot jump conditions. Most of the theoretical work was done in the mid-twentieth century. Ribner (1954) studied the interaction of vorticity and a shock wave, in which an arbitrary weak spatial distribution of vorticity was represented in terms of plane sinusoidal shear waves. He analysed the interaction between a single representative weak shear wave and a shock wave by LIA. It was found that a sinusoidal shear wave passing into the shock wave at an arbitrary inclination gives rise to a downstream shear wave of altered inclination and amplitude. Moore (1954) investigated the oblique impingement of three kinds of plane disturbance on a plane-normal shock wave: (1) a shock wave overtaking sound waves, (2) sound waves overtaking a shock wave from behind and (3) a shock wave overtaking a stationary shear wave. It was found that the refraction characteristics of sound waves and vorticity waves depend on the angle between the shock wave and the incident wave. Kerrebrock (1956) studied the interaction of three types of disturbance, namely pressure, entropy and vorticity. It was found that all three types of disturbance are generated in comparable strengths in downstream flow by their presence in the upstream flow. D'iakov (1958*a*,*b*) considered their interactions in supersonic and subsonic post-shock flows. When the flow after the shock wave is supersonic, it was found that linearized approximations break down at a certain incident flow Mach number; while, when the flow after the shock wave is subsonic, linearized approximations always break down, as they predict singularities. On the basis of this study, McKenzie & Westphal (1968) provided a relatively complete solution to this problem that describes the dependences of the transmission, reflection and generation sound wave coefficients on the Mach number and angles of incidence for all types of disturbance. They also found that there is a critical angle downstream of an oblique shock wave at which acoustic disturbances are excited; however, they did not provide a result for the critical angle when no acoustic waves are generated behind the shock wave. Robinet & Casalis (2001) deemed that this critical angle may appear as a singularity in linearized Euler equations.

Another approach is numerical simulation, especially direct numerical simulation (DNS). Besides the high-order shock-fitting method (Zhong 1998), many high-resolution shock-capturing schemes have been proposed, such as essentially non-oscillatory (ENO) (Shu & Osher 1988) and weighted essentially non-oscillatory

(WENO) (Jiang & Shu 1996), such that DNS has become a major tool for studying these interactions. Lee, Lele & Moin (1993) studied the interaction of isotropic turbulence with a weak normal shock wave by DNS and investigated the effects of a fluctuating Mach number in the upstream turbulence and shock strength on turbulence. It was found that turbulence is enhanced during interaction with a shock wave and the distortion of the shock wave is closely related to Mach-number fluctuation. Based on this outstanding work, a series of DNS studies on the interaction between isotropic turbulence and shock waves were conducted. They considered various factors, such as the effect of shock strength (Lee, Lele & Moin 1997), various types of isotropic turbulence (Jamme *et al.* 2002), instantaneous interaction (Larsson & Lele 2009), the effects of Reynolds and Mach numbers (Larsson, Bermejo-Moreno & Lele 2013), vortical isotropic turbulence (Ryu & Livescu 2014) and variable-density turbulence (Tian *et al.* 2017). Most DNS results agree well with those obtained by LIA, and many new phenomena have been reasonably explained, thereby improving the understanding of the shock–turbulence interaction (STI).

According to previous studies, the interaction between disturbances and shock waves has been well described by LIA and great progress in describing STI has been made by DNS. However, an unsolved theoretical problem remains. Moore (1954) pointed out that an attenuating isentropic pressure wave will be excited under a certain condition. Most previous studies identified the existence of two critical angles, but what happens between the two critical angles remains unclear. Because this condition does not occur for a normal shock wave, this problem does not involve STI, in which the shock wave is nominally normal. The present study focuses on this problem, and the concept of a damped wave is proposed for cases where no acoustic waves are generated. Based on a theoretical LIA approach, the dispersion and amplitude relationships of a plane wave across a shock wave are presented analytically, systematically and comprehensively.

Typically, there are two kinds of shock wave over supersonic/hypersonic vehicles: (1) a bow shock wave ahead and proximate to the leading edge and (2) an oblique shock wave over the head/body of the vehicle. The former is very complicated due to the curvature of the shape of the shock wave. The latter is simpler because the disturbances passing through the shock wave can be treated as a one-dimensional problem. In this paper we focus on an oblique shock wave, while a bow shock wave will be addressed in our next paper.

The rest of the paper is organized as follows. In § 2, we describe the problem and the formulation in detail. The governing equations of the base flow and disturbances away from and across an oblique shock wave are presented. A damped wave is introduced as a type of plane wave in a uniform and homogeneous flow field. The dispersion relationship of a plane wave across an oblique shock wave is constructed by introducing two universal wavenumbers. The angle limitation of an incident plane wave and the existence of critical angles are clarified. The amplitude relationship between any incident plane wave and stimulated waves are constructed analytically. In § 3, our results are verified using theoretical and DNS results. In § 4, the physical essence of a damped wave is analysed, and the contribution of each type of wave to the amplitude of the excited disturbance is evaluated. Engineering applications are also discussed. Finally, § 5 summarizes the main conclusions.

2. Problem description and formulation

2.1. *Governing equations*

Figure 1(*a*) shows the physical model to be studied, in which a two-dimensional (2-D) linear disturbance passes through an oblique shock wave. In the 2-D Cartesian

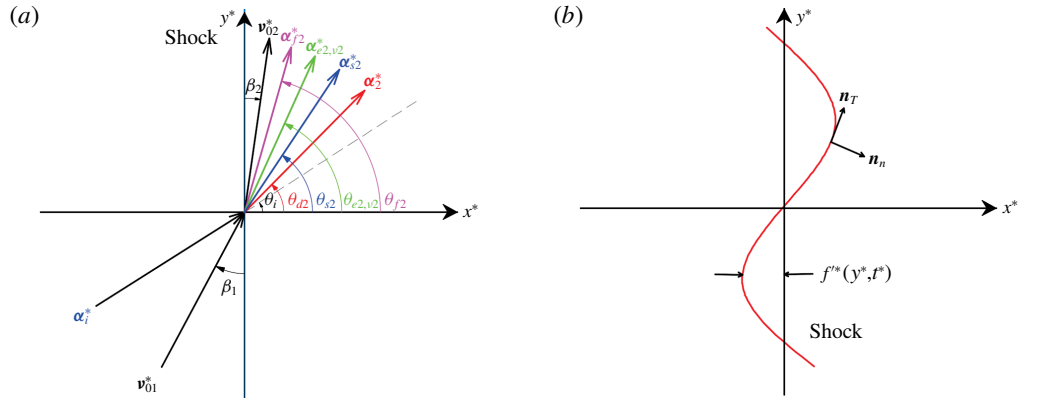

FIGURE 1. (Colour online) Sketch maps of (*a*) the physical model and (*b*) the shock deformation.

coordinate system (x^*, y^*), the undisturbed shock wave is fixed at the y^* axis and the flow field is divided into two regions. Flow is indicated by subscript 1 before the shock wave and by subscript 2 after it. Superscript $*$ represents dimensional variables.

2.1.1. *Governing equation of flow before and after an oblique shock wave*

In the interaction between disturbances and an oblique shock wave, the viscosity is too weak to be ignored. Hence the flow before and after the shock wave is governed by the inviscid Euler equation

$$\frac{\partial \boldsymbol{U}_p^*}{\partial t^*} + \frac{\partial \boldsymbol{E}^*}{\partial x^*} + \frac{\partial \boldsymbol{F}^*}{\partial y^*} = \boldsymbol{0}, \tag{2.1}$$

where

$$\boldsymbol{U}_p^* = \begin{pmatrix} \rho^* \\ \rho^* u^* \\ \rho^* v^* \\ \rho^* h^* - p^* \end{pmatrix}, \quad \boldsymbol{E}^* = \begin{pmatrix} \rho^* u^* \\ \rho^* u^* u^* + p^* \\ \rho^* u^* v^* \\ \rho^* u^* h^* \end{pmatrix}, \quad \boldsymbol{F}^* = \begin{pmatrix} \rho^* v^* \\ \rho^* v^* u^* \\ \rho^* v^* v^* + p^* \\ \rho^* v^* h^* \end{pmatrix}. \tag{2.2a–c}$$

In these equations, t^* is the time variable; ρ^*, u^*, v^*, p^* denote the density, velocities in the x^* and y^* directions, and pressure, respectively; $h^* = e^* + (\gamma p^*/\rho^*)/(\gamma - 1)$ is the total enthalpy; $e^* = (u^{*2} + v^{*2})/2$ is the kinetic energy; γ is the specific heat ratio; $\boldsymbol{U}_p^*$ is the conservative flux; and $\boldsymbol{E}^*$ and $\boldsymbol{F}^*$ are the convective fluxes in the x^* and y^* directions, respectively.

Supposing that the base flow in the uniform and homogeneous field is steady, the base flow $\boldsymbol{U}_0^* = [\rho_0^*, u_0^*, v_0^*, p_0^*]^{\mathrm{T}}$ is governed by (2.1) but is independent of the coordinates (x^*, y^*) and time t^*, where the subscript 0 represents the undisturbed base flow. As shown in figure 1(*a*), when the incoming base flow with the velocity vector $\boldsymbol{v}_{01}^* = (u_{01}^*, v_{01}^*)$ passes through an oblique shock wave, it yields the base flow with the velocity vector $\boldsymbol{v}_{02}^* = (u_{02}^*, v_{02}^*)$ after the shock wave. Different from the normal shock wave, which is perpendicular to the direction of the incoming base flow, there is a shock wave angle between the oblique shock wave and the incoming base flow, which is defined as $\beta_1 \subset (0, \pi)$. Notably, an oblique shock wave returns to a normal

shock wave when $\beta_1 = \pi/2$. Because of the inclination characteristic, the flow will be deflected by an oblique shock wave, leading to an angle β_2 between the oblique shock wave and the base flow after the shock wave.

A weak disturbance in a free stream can be expressed in the form of a normal mode as

$$\boldsymbol{U}'^* = [\rho'^*, u'^*, v'^*, p'^*]^{\mathrm{T}} = \hat{a}\boldsymbol{C}^* \exp(-\alpha_d^* x^*) \exp(\mathrm{i}\Theta^*) + \text{c.c.}, \tag{2.3}$$

where

$$\Theta^* = \alpha_x^* x^* + \alpha_y^* y^* - \omega^* t^*, \quad \boldsymbol{C}^* = [\hat{\rho}^*, \hat{u}^*, \hat{v}^*, \hat{p}^*]^{\mathrm{T}}. \tag{2.4a,b}$$

Here $\boldsymbol{\alpha}^* = (\alpha_x^*, \alpha_y^*)$, ω^* and $\hat{a}$ denote the wavenumber vector, circle frequency and amplitude of the disturbance, respectively; α_d^* is the decay rate of the amplitude satisfying $\alpha_d^* \geqslant 0$; Θ^* and $\boldsymbol{C}^*$ are the phase and shape function of the perturbation; and c.c. stands for complex conjugate.

Unlike the classical normal mode (Reshotko 1976) in which the wavenumber vector $\boldsymbol{\alpha}^*$ can be a complex number and its imaginary component can describe the variation in amplitude, the wavenumber vector $\boldsymbol{\alpha}^* = (\alpha_x^*, \alpha_y^*)$ in (2.3) is a real number, and a new real parameter α_d^* is introduced to describe the variation in amplitude, through which the damped wave concept can be introduced clearly.

When the base flow $\boldsymbol{U}_0^*$ is perturbed by a small-amplitude disturbance $\boldsymbol{U}'^*$, the total flow is $\boldsymbol{U}^* = \boldsymbol{U}_0^* + \boldsymbol{U}'^*$. Both the base flow and the total flow satisfy the inviscid Euler equation. Applying the total flow to the governing equation and linearizing with the base flow, one can obtain the linearized disturbance equation governing the disturbance $\boldsymbol{U}'^*$, which can be written in the following form:

$$\Gamma(\alpha_x^*, \alpha_y^*, \omega^*, \alpha_d^*; \boldsymbol{U}_0^*)\boldsymbol{C}^* = \boldsymbol{0}. \tag{2.5}$$

Here Γ is an operator through which the wave parameters α_x^*, α_y^*, ω^*, α_d^* and the shape function $\boldsymbol{C}^*$ are determined for a given base flow $\boldsymbol{U}_0^*$.

Typically there are four types of small disturbance in (2.5): fast acoustic wave, slow acoustic wave, entropy wave and vorticity wave. Any type of disturbance striking a shock wave may generate all four types of wave behind the shock wave. However, as mentioned later, we find that another type of wave can be stimulated behind the shock wave by an incident wave under a certain condition. It is called a damped wave because its amplitude decays along the propagation direction. As shown in figure 1(*a*), the vector $\boldsymbol{\alpha}_i^*$ with wave angle θ_i is an arbitrary incident wavevector before or after the shock wave, while the vectors $\boldsymbol{\alpha}_{f2}^*$, $\boldsymbol{\alpha}_{s2}^*$, $\boldsymbol{\alpha}_{e2}^*$, $\boldsymbol{\alpha}_{v2}^*$ and $\boldsymbol{\alpha}_{d2}^*$ are the stimulated wavevectors of the fast acoustic wave, slow acoustic wave, entropy wave, vorticity wave and damped wave behind the shock wave, respectively, whose corresponding wave angles are θ_{f2}, θ_{s2}, θ_{e2}, θ_{v2} and θ_{d2}.

2.1.2. *Governing equation of base flow across an oblique shock wave*

The condition that must be satisfied across a discontinuity is that the normal mass flux, momentum and energy are all continuous. Thus, the so-called Rankine–Hugoniot (RH) condition (McKenzie & Westphal 1968) can be written as

$$\boldsymbol{E}_1^*(\rho^*, u^*, v^*, p^*)|_{x_s^*} = \boldsymbol{E}_2^*(\rho^*, u^*, v^*, p^*)|_{x_s^*}, \tag{2.6}$$

where x_s^* is the location of the shock wave, $\boldsymbol{E}^*$ is the convective flux in the x^* direction, and u^* and v^* are the velocities perpendicular and parallel to the shock wave, respectively. If the unperturbed discontinuity is an oblique shock wave located at $x_s^* = 0$, the unperturbed base flow on either side of the shock wave satisfies the RH condition, namely

$$\boldsymbol{E}_1^*(\rho_{01}^*, u_{01}^*, v_{01}^*, p_{01}^*)|_{x_s^*=0} = \boldsymbol{E}_2^*(\rho_{02}^*, u_{02}^*, v_{02}^*, p_{02}^*)|_{x_s^*=0}. \tag{2.7}$$

2.1.3. *Governing equation of disturbance across an oblique shock wave*

For a steady oblique shock, it is necessary to consider the shock deformation caused by a small inlet disturbance when studying the interaction between the disturbance and the shock wave, as shown in figure 1(*b*). Supposing that an oblique shock wave is located in the plane $x_s^* = 0$, the deformation of the shock wave may be written as

$$x^* = f'^*(y^*, t^*), \quad \text{where } f'^* \ll 1, \tag{2.8}$$

through which the velocity vector $\boldsymbol{u}_d'^*$ of the distorted shock wave and the velocity vector $\boldsymbol{u}_r^*$ of the fluid relative to the shock wave can be given by

$$\boldsymbol{u}_d'^* = \left(\frac{\partial f'^*}{\partial t^*} + \frac{\partial f'^*}{\partial y^*}\frac{\mathrm{d}y^*}{\mathrm{d}t^*}, \frac{\mathrm{d}y^*}{\mathrm{d}t^*}\right), \quad \boldsymbol{u}_r^* = \boldsymbol{u}_0^* + \boldsymbol{u}'^* - \boldsymbol{u}_d'^*. \tag{2.9a,b}$$

When the incident perturbation is a plane harmonic wave of the form $\exp(\mathrm{i}\Theta^*)$, one can take the deformation f'^* to be of the same form (McKenzie & Westphal 1968):

$$f'^*(y^*, t^*) = \hat{f}^* \exp(\mathrm{i}\Psi^*) + \text{c.c.}, \quad \text{with } \Psi^* = \alpha_y^* y^* - \omega^* t^*, \tag{2.10}$$

where $\hat{f}^*$ is the amplitude of the shock distortion, which is to be determined from the boundary conditions. Then, the velocity components of the fluid relative to the shock wave are

$$u_r^* = \boldsymbol{u}_r^* \cdot \boldsymbol{n}_N = u_0^* + u'^* + v_0^*\frac{\alpha_y^*}{\omega^*}u_d'^* - u_d'^*, \quad v_r^* = \boldsymbol{u}_r^* \cdot \boldsymbol{n}_T = v_0^* + v'^* - u_0^*\frac{\alpha_y^*}{\omega^*}u_d'^* - \frac{\mathrm{d}y^*}{\mathrm{d}t^*}, \tag{2.11a,b}$$

where

$$u_d'^* = \frac{\partial f'^*}{\partial t^*} = \hat{u}_d^* \exp(\mathrm{i}\Psi^*) + \text{c.c.}, \quad \boldsymbol{n}_N \approx \left(1, -\frac{\partial f'^*}{\partial y^*}\right), \quad \boldsymbol{n}_T \approx \left(\frac{\partial f'^*}{\partial y^*}, 1\right), \tag{2.12a–c}$$

in which $u_d'^*$ is the x^* component of $\boldsymbol{u}_d'^*$, $\hat{u}_d^*$ is its amplitude, and $\boldsymbol{n}_N$ and $\boldsymbol{n}_T$ are unit vectors normal and tangential to the deformed shock wave, respectively.

Since the incident plane wave has a small amplitude, in the linear approximation, the perturbed flow on either side of the shock wave also satisfies the RH condition, namely

$$\boldsymbol{E}_1^*(\rho_1^*, u_{r1}^*, v_{r1}^*, p_1^*)|_{x_s^*=f'^*} = \boldsymbol{E}_2^*(\rho_2^*, u_{r2}^*, v_{r2}^*, p_2^*)|_{x_s^*=f'^*}, \tag{2.13}$$

where $\rho^* = \rho_0^* + \rho'^*$ and $p^* = p_0^* + p'^*$ are the density and pressure of the disturbed flow, and $\boldsymbol{v}_r^* = (u_r^*, v_r^*)$ is a velocity vector of the fluid relative to the shock wave. Furthermore, the frequency ω^* and the y^* component of the wavevector $\boldsymbol{\alpha}^*$ will be continuous, namely

$$\omega_1^* = \omega_2^*, \quad \alpha_{y1}^* = \alpha_{y2}^*. \tag{2.14a,b}$$

Linearizing the RH condition of disturbed flow about the unperturbed flow in (2.13) at $x_s^* = 0$, one can obtain the linear RH condition governing the perturbation $\boldsymbol{U}'^*$. For the ensuing analysis, it is convenient to cast it into the matrix form:

$$\boldsymbol{A}_1^*(\boldsymbol{U}_1'^* - \boldsymbol{C}_{b1}^* u_d'^*)|_{x_s^*=0} = \boldsymbol{A}_2^*(\boldsymbol{U}_2'^* - \boldsymbol{C}_{b2}^* u_d'^*)|_{x_s^*=0}, \tag{2.15}$$

where the coefficients $\boldsymbol{A}^*$ and $\boldsymbol{C}_b^*$ can be found in appendix A.

2.2. *Plane wave in a uniform and homogeneous field*

For convenience, the flow variables before and after an oblique shock wave are non-dimensionalized by the steady-state free-stream conditions before and after the shock wave, respectively. Namely, the reference parameters before the shock wave are ρ_{01}^*, u_{01}^* and d^*, and those after the shock wave are ρ_{02}^*, u_{02}^* and d^*. Here, we use the same reference length d^*. So the non-dimensional variables of the undisturbed base flow are

$$\boldsymbol{U}_0 = [\rho_0, u_0, v_0, p_0]^{\mathrm{T}} = \left[1, 1, \frac{\cos\beta}{\sin\beta}, \frac{1}{\gamma M_n^2}\right]^{\mathrm{T}}, \tag{2.16}$$

where $M_n = M\sin\beta$ is the normal Mach number defined by the velocity perpendicular to the shock wave, $M = \sqrt{u_0^{*2} + v_0^{*2}}/c_0^*$ is the Mach number of free-stream flow, β is the shock wave angle and $c_0^* = \sqrt{\gamma p_0^*/\rho_0^*}$ is the speed of sound.

Based on (2.5), the non-dimensional linearized disturbance equation can be written in the matrix form

$$\begin{bmatrix} \chi & \alpha_x + \mathrm{i}\alpha_d & \alpha_y & 0 \\ 0 & \chi & 0 & \alpha_x + \mathrm{i}\alpha_d \\ 0 & 0 & \chi & \alpha_y \\ 0 & (\alpha_x + \mathrm{i}\alpha_d)/M_n^2 & \alpha_y/M_n^2 & \chi \end{bmatrix} \begin{bmatrix} \hat{\rho} \\ \hat{u} \\ \hat{v} \\ \hat{p} \end{bmatrix} = \begin{bmatrix} 0 \\ 0 \\ 0 \\ 0 \end{bmatrix}, \tag{2.17}$$

whose dispersion relationship satisfies

$$\chi^2 \left[\chi^2 - \frac{(\alpha_x + \mathrm{i}\alpha_d)^2 + \alpha_y^2}{M_n^2}\right] = 0, \tag{2.18}$$

where we have put

$$\chi = \alpha_x + \mathrm{i}\alpha_d + v_0\alpha_y - \omega. \tag{2.19}$$

When the decay rate of the amplitude is zero, namely, $\alpha_d = 0$, solving the above dispersion relation (2.18), one can obtain typical solutions for the fast acoustic wave, slow acoustic wave, entropy wave and vorticity wave written in the united form as

$$\omega = \left(\sin(\theta + \beta) + \frac{\sigma}{M}\right)\frac{\alpha}{\sin\beta}, \quad \text{where } \sigma = \begin{cases} 1, & \text{fast acoustic wave,} \\ 0, & \text{entropy–vorticity wave,} \\ -1, & \text{slow acoustic wave,} \end{cases} \tag{2.20}$$

where $\theta \subseteq [-\pi, \pi)$ is the wave angle and $\alpha = \sqrt{\alpha_x^2 + \alpha_y^2} > 0$ is the wavenumber, with $\alpha_x = \alpha\cos\theta$ and $\alpha_y = \alpha\sin\theta$ the components of wavenumber vector $\boldsymbol{\alpha}$ in the x and y directions, respectively.

When the amplitude decay rate is greater than zero, namely, $\alpha_d > 0$, solving the dispersion relation (2.18), one can obtain the special solution for a damped wave:

$$\omega = \frac{M_n^2 - 1}{M_n^2}\alpha_x + v_0\alpha_y, \quad \alpha_d = \sqrt{\frac{\alpha_y^2}{1 - M_n^2} - \frac{\alpha_x^2}{M_n^2}}, \tag{2.21a,b}$$

under the condition

$$\frac{\alpha_y^2}{1 - M_n^2} > \frac{\alpha_x^2}{M_n^2}, \tag{2.22}$$

from which it can be seen that a damped wave cannot exist before the shock wave but may appear after it. A damped wave usually cannot be discovered in a uniform and homogeneous field because its amplitude of oscillation decreases along the propagation direction, eventually becoming zero. However, it is an important physical part of post-shock excited waves.

The corresponding eigenvector of the solution in (2.18) for the five types of wave can be written in the united form as

$$\left.\begin{array}{ll} \boldsymbol{C}_f = [M_n^2,\, M_n\cos\theta_f,\, M_n\sin\theta_f,\, 1]^{\mathrm{T}}, & \text{fast acoustic wave,} \\ \boldsymbol{C}_s = [M_n^2,\, -M_n\cos\theta_s,\, -M_n\sin\theta_s,\, 1]^{\mathrm{T}}, & \text{slow acoustic wave,} \\ \boldsymbol{C}_e = [1,\, 0,\, 0,\, 0]^{\mathrm{T}}, & \text{entropy wave,} \\ \boldsymbol{C}_v = [0,\, -\sin\theta_v,\, \cos\theta_v,\, 0]^{\mathrm{T}}, & \text{vorticity wave,} \\ \boldsymbol{C}_d = [M_n^2,\, -M_n g_x,\, -M_n g_y,\, 1]^{\mathrm{T}}, & \text{damped wave,} \end{array}\right\} \tag{2.23}$$

where $\cos\theta = \alpha_x/\sqrt{\alpha_x^2+\alpha_y^2}$, $\sin\theta = \alpha_y/\sqrt{\alpha_x^2+\alpha_y^2}$, $g_x = (\alpha_x+\mathrm{i}\alpha_d)/\sqrt{(\alpha_x+\mathrm{i}\alpha_d)^2+\alpha_y^2}$, $g_y = \alpha_y/\sqrt{(\alpha_x+\mathrm{i}\alpha_d)^2+\alpha_y^2}$, and subscripts f, s, e, v and d represent the fast acoustic wave, slow acoustic wave, entropy wave, vorticity wave and damped wave, respectively. The amplitude of the fast acoustic/slow acoustic/damped wave is defined as the amplitude of the pressure fluctuation, while the amplitudes of the entropy and vorticity waves are defined as the amplitudes of the density and velocity fluctuations, respectively.

The group velocity for four typical types of wave can be written in the united form as

$$\boldsymbol{u}_g = (u_{gx},\, u_{gy}) = \left(\frac{\partial\omega}{\partial\alpha_x},\, \frac{\partial\omega}{\partial\alpha_y}\right) = \left(1+\frac{\sigma\cos\theta}{M_n},\, \frac{\cos\beta}{\sin\beta}+\frac{\sigma\sin\theta}{M_n}\right), \tag{2.24}$$

where the energy of the corresponding wave propagates from upstream to downstream when $u_{gx}>0$, while the energy of the wave with a negative u_{gx} value propagates from downstream to upstream.

The group velocity for a damped wave is

$$\boldsymbol{u}_g = (u_{gx},\, u_{gy}) = \left(\frac{\partial\omega}{\partial(\alpha_x+\mathrm{i}\alpha_d)},\, \frac{\partial\omega}{\partial\alpha_y}\right)_r = \left(1+\frac{\sigma g_x}{M_n},\, \frac{\cos\beta}{\sin\beta}+\frac{\sigma g_y}{M_n}\right)_r, \tag{2.25}$$

where subscript r means the real part. It can be proven that u_{gx} is always positive, indicating that the energy of the excited damped wave always propagates downstream when it is excited by an incident plane wave.

2.3. *Dispersion relationship of a plane wave across an oblique shock wave*

Based on (2.7), it easy to obtain the relationships of the base flow before and after the shock wave, as follows:

$$v_{01} = u_b v_{02}, \quad M_{n1}^2 = \frac{2}{u_b(\gamma+1)-(\gamma-1)}, \quad M_{n2}^2 = \frac{2u_b}{(\gamma+1)-u_b(\gamma-1)}. \tag{2.26a–c}$$

Here we prefer to use u_b defined as follows to describe the relationship conveniently:

$$u_b = \frac{u_{02}^*}{u_{01}^*} = \frac{2+(\gamma-1)M_{n1}^2}{(\gamma+1)M_{n1}^2} \in \left(\frac{\gamma-1}{\gamma+1},\, 1\right). \tag{2.27}$$

In order to conveniently study the interaction of plane waves and an oblique shock wave, we define two universal kinds of wavenumber for the excited wave as

$$\alpha_q \equiv \omega_2 - v_{02}\alpha_{y2}, \quad \alpha_p \equiv \alpha_{y2}, \tag{2.28a,b}$$

where α_q is an equivalent wavenumber perpendicular to the surface of the shock wave, while α_p is a wavenumber parallel to it.

Based on (2.14), one can obtain the non-dimensional continuity condition for the frequency ω and the wavenumber α_y as

$$\omega_1 = u_b\omega_2, \quad \alpha_{y1} = \alpha_{y2}. \tag{2.29a,b}$$

Substituting (2.28) and (2.29) into (2.20), one can obtain the following relationship for four classical types of wave before and after the shock wave:

$$\left(\cos\theta_1 + \frac{\sigma_1}{M_{n1}}\right)\frac{\alpha_1}{u_b} = \left(\cos\theta_2 + \frac{\sigma_2}{M_{n2}}\right)\alpha_2 = \alpha_q, \quad \alpha_1\sin\theta_1 = \alpha_2\sin\theta_2 = \alpha_p. \tag{2.30a,b}$$

On the one hand, for any incident plane wave with frequency ω_i and wave angle θ_i, whose wavenumber α_i is determined by the dispersion relationship in (2.20), one can obtain the values of α_p and α_q according to (2.30), whether the incident plane wave is ahead of the shock wave (denoted by subscript 1) or behind it (denoted by subscript 2).

On the other hand, the wavenumber α_2 and wave angle θ_2 of the excited wave after the shock wave are also governed by (2.30) for given values of α_p and α_q, and its corresponding wave frequency is determined by (2.20). The solution of (2.30) for given values of α_p and α_q is

$$\alpha_2 = \frac{\alpha_q^2 + \alpha_p^2}{\alpha_q\sigma_2/M_{n2} \pm \sqrt{\Delta_2}}, \quad \theta_2 = \left(\theta_{A2} + \frac{\pi}{2}\right) \pm \left(\sigma_2\theta_{B2} - \frac{\pi}{2}\right), \tag{2.31a,b}$$

under the condition

$$\alpha_2 > 0 \quad \text{and} \quad \Delta_2 = \alpha_q^2 + (1 - \sigma_2^2/M_{n2}^2)\alpha_p^2 \geqslant 0, \tag{2.32a,b}$$

where we have put

$$\sin\theta_{A2} = \frac{\alpha_p}{\sqrt{\alpha_q^2 + \alpha_p^2}}, \quad \cos\theta_{A2} = \frac{\alpha_q}{\sqrt{\alpha_q^2 + \alpha_p^2}}, \quad \theta_{B2} = \arcsin\frac{\alpha_p/M_{n2}}{\sqrt{\alpha_q^2 + \alpha_p^2}} \in \left[-\frac{\pi}{2}, \frac{\pi}{2}\right]. \tag{2.33a–c}$$

Substituting the solution in (2.31) into (2.24), one can obtain the x component of the group velocity vector of the excited wave after the shock wave as

$$u_{gx2} = \frac{\sqrt{\Delta_2}(\sqrt{\Delta_2} \pm \alpha_q\sigma_2/M_{n2})}{\alpha_q^2 + \alpha_p^2}, \tag{2.34}$$

where u_{gx2} has the same positive/negative characteristics as the $\pm$ sign. A positive u_{gx2} value indicates that the excited wave is initiated at the position of the shock wave and its energy propagates downstream. Meanwhile, the energy of the stimulated wave,

whose u_{gx2} value is negative, propagates from downstream towards the shock wave, implying that this wave is a non-physical solution for the excited wave, and that the negative component of the $\pm$ sign in (2.31) should be abandoned.

Substituting (2.28) into (2.21), one can obtain the following relationship for a damped wave:

$$\alpha_{x2} = \frac{M_{n2}^2}{M_{n2}^2 - 1}\alpha_q, \quad \alpha_{y2} = \alpha_p, \tag{2.35a,b}$$

whose solution is

$$\alpha_{d2} = \frac{1}{1 - M_{n2}^2}\sqrt{(1 - M_{n2}^2)\alpha_p^2 - M_{n2}^2\alpha_q^2}, \tag{2.36a}$$

$$\sin\theta_{d2} = \frac{(1 - M_{n2}^2)\alpha_p}{\sqrt{M_{n2}^4\alpha_q^2 + (1 - M_{n2}^2)^2\alpha_p^2}}, \quad \cos\theta_{d2} = \frac{-M_{n2}^2\alpha_q}{\sqrt{M_{n2}^4\alpha_q^2 + (1 - M_{n2}^2)^2\alpha_p^2}}. \tag{2.36b,c}$$

2.4. *Angle limitations*

2.4.1. *Angle limitation of base flow*

The base flow before the oblique shock wave must be supersonic, namely, $M_1 > 1$ and $M_{n1} = M_1 \sin\beta_1 > 1$, which produces the limitation for β_1 as

$$\beta_1 \in (\beta_{m1},\ \pi - \beta_{m1}), \quad \text{where } \beta_{m1} = \arcsin\frac{1}{M_1}. \tag{2.37}$$

The base flow after the oblique shock wave can be supersonic ($M_2 > 1$) or subsonic ($M_2 < 1$), while, of course, $M_{n2} < 1$, which determines the limitation for β_2 as

$$\left.\begin{array}{ll} \beta_2 \in (0,\ \beta_{m2}) \cup (\pi - \beta_{m2},\ \pi) & \text{when } M_2 > 1, \\ \beta_2 \in (0,\ \pi) & \text{when } M_2 < 1, \end{array}\right\} \quad \text{where } \beta_{m2} = \arcsin\frac{1}{M_2}. \tag{2.38}$$

2.4.2. *Angle limitation of plane wave*

In mathematics, the value of frequency ω in (2.20) can be positive or negative; however, this would lead to ambiguity in the definitions of the fast and slow acoustic waves. For example, a slow acoustic wave with wave angle θ_s and a negative frequency $-\omega$ is the same as a fast acoustic wave with wave angle θ_f and a positive frequency ω, where their wave angles satisfy the relationship $\sin(\theta_f + \beta) + \sin(\theta_s + \beta) = 0$.

In physics, frequency is defined as a number of cycles per unit time and usually has a positive value. So, the fundamental limitation for a plane wave is that the frequency in (2.20) should be greater than zero, indicating that the angle of the plane wave is limited to

$$\sin(\theta + \beta) > -\frac{\sigma}{M}, \tag{2.39}$$

whose result is shown in table 1, where β_m is the Mach angle and β_n is the normal Mach angle defined as

$$\left.\begin{array}{ll} \beta_m = \arcsin\dfrac{1}{M} \in (0,\ \pi/2), & \text{when } M > 1, \\ \beta_n = \arccos M_n \in (0,\ \pi/2), & \text{when } M_n < 1. \end{array}\right\} \tag{2.40}$$

Condition	Flow type	θ_f	$\theta_e,\ \theta_v$	θ_s
$\omega > 0$	$M < 1$	$[-\pi, \pi]$	$(-\beta, \pi - \beta)$	$\varnothing$
$\omega > 0$	$M > 1$	$(-\beta_m - \beta, \pi + \beta_m - \beta)$	$(-\beta, \pi - \beta)$	$(\beta_m - \beta, \pi - \beta_m - \beta)$
$u_{gx} > 0$	$M_n < 1$	$(-\pi + \beta_n, \pi - \beta_n)$	$[-\pi, \pi]$	$[-\pi, -\beta_n) \cup (\beta_n, \pi]$
$u_{gx} > 0$	$M_n > 1$	$[-\pi, \pi]$	$[-\pi, \pi]$	$[-\pi, \pi]$
$u_{gx} < 0$	$M_n < 1$	$[-\pi, -\pi + \beta_n) \cup (\pi - \beta_n, \pi]$	$\varnothing$	$(-\beta_n, \beta_n)$
$u_{gx} < 0$	$M_n > 1$	$\varnothing$	$\varnothing$	$\varnothing$

TABLE 1. Wave angle limitation of plane wave, where $\beta_m = \arcsin(1/M)$ is the Mach angle when $M > 1$, and $\beta_n = \arccos M_n$ is the normal Mach angle when $M_n < 1$.

From table 1, the wave angle limitation of the entropy–vorticity wave in subsonic flow has the same form as that in supersonic flow, indicating that the existence of an entropy–vorticity wave is independent of the flow condition. For subsonic flow, namely, when $M < 1$, there is no slow acoustic wave angle that satisfies limitation equation (2.39), implying that a slow acoustic wave does not exist in subsonic flow. Meanwhile, any fast acoustic wave angle satisfies the condition of (2.39), indicating that the fast acoustic wave always exists in subsonic flow. When the flow is supersonic, namely, when $M > 1$, the fast and slow acoustic waves can coexist, with the fast acoustic wave having a larger range of wave angles.

In addition, the angle of a plane wave should be also restricted by (2.24), whose result is also given in table 1. When $u_{gx} > 0$, there is no limitation for the entropy–vorticity wave, implying that it can always exist before and after the shock wave. Similarly, the fast and slow acoustic waves can always exist before the shock wave when $M_n > 1$, and can also exist after the shock wave within a certain range of wave angles when $M_n > 1$. When $u_{gx} < 0$, there is no plane wave propagating upstream before the shock wave. Only the fast and slow acoustic waves can exist and propagate upstream after the shock wave, but they cannot coexist because their ranges of wave angle limitation are mutually exclusive after the shock wave.

2.4.3. *Angle limitation of incident plane wave*

An incident plane wave has more strictly limited wave angles than an ordinary plane wave, as it should propagate towards the shock wave. Specifically, an incident plane wave before the shock wave should propagate downstream to the shock wave, while one behind the shock wave should propagate upstream towards it. This section addresses in more detail the angle limitations of an incident plane wave in the excitation of the fast acoustic/slow acoustic/damped waves.

Based on (2.32) and (2.22), one can obtain the conditions needed to excite each type of plane wave:

$$\left.\begin{array}{rl} \varnothing, & \text{entropy–vorticity wave,} \\ \alpha_q \geqslant \sqrt{1/M_{n2}^2 - 1}|\alpha_p|, & \text{fast acoustic wave,} \\ \alpha_q \leqslant -\sqrt{1/M_{n2}^2 - 1}|\alpha_p|, & \text{slow acoustic wave,} \\ |\alpha_q| < \sqrt{1/M_{n2}^2 - 1}|\alpha_p|, & \text{damped wave.} \end{array}\right\} \tag{2.41}$$

On the one hand, equation (2.41) describes the possibility and conditions needed to excite each type of plane wave after the shock wave. The entropy–vorticity wave

can always be stimulated by an incident plane wave without any limitation. The fast and slow acoustic waves cannot be excited at the same time by an incident plane wave because their excitation conditions oppose each other. A damped wave will be stimulated after the shock wave by an incident plane wave when neither the fast nor slow acoustic waves are excited.

On the other hand, equation (2.41) also limits the universal wavenumbers α_p and α_q, through which the wave angle of the incident plane wave is limited at the same time. One can apply the conditions in (2.41) to (2.30) to obtain the wave angle limitation of the incident plane wave.

If the incident plane wave is ahead of the shock wave, its wave angle should satisfy conditions $\omega > 0$ and $u_{gx} > 0$ at the same time (table 1), which can be written in a united form as

$$\theta_{i1} \in (-\sigma_1\beta_{m1} - \beta_1,\ \pi + \sigma_1\beta_{m1} - \beta_1). \tag{2.42}$$

Applying (2.41) to (2.30) yields an additional limitation on the incident wave angle before the shock wave needed to excite the fast acoustic/slow acoustic/damped wave:

$$\theta_{i1} \in \begin{cases} [-\theta_{cf},\ \theta_{cf}], & \text{fast acoustic wave,} \\ [-\pi,\ -\theta_{cs}] \cup [\theta_{cs},\ \pi], & \text{slow acoustic wave,} \\ (-\theta_{cs},\ -\theta_{cf}) \cup (\theta_{cf},\ \theta_{cs}), & \text{damped wave,} \end{cases} \tag{2.43}$$

in which θ_{cf} and θ_{cs} are the critical angles needed to excite the fast and slow acoustic waves, respectively. They are defined as

$$\theta_{cf} = \theta_{Ac} + \sigma_1\theta_{Bc}, \quad \theta_{cs} = \pi - \theta_{Ac} + \sigma_1\theta_{Bc}, \tag{2.44a,b}$$

where we have put

$$\theta_{Ac} = \arcsin\frac{1}{\sqrt{1+s^2}} \in \left[\arcsin\sqrt{\frac{8}{\gamma+9}},\ \frac{\pi}{2}\right), \quad \theta_{Bc} = \arcsin\frac{1}{M_{n1}\sqrt{1+s^2}} \in \left(0,\ \frac{\pi}{2}\right), \tag{2.45a,b}$$

$$s = \sqrt{\frac{\gamma+1}{2}u_b(1-u_b)} \in \left(0,\ \sqrt{\frac{\gamma+1}{8}}\right]. \tag{2.45c}$$

If the incident plane wave is behind the shock wave, its wave angle should satisfy the conditions $\omega > 0$ and $u_{gx} < 0$ at the same time. From table 1, it can be seen that the range of wave angles for entropy–vorticity waves is empty when $u_{gx} < 0$, indicating that the incident plane wave behind the shock wave cannot be an entropy or vorticity wave.

The fast acoustic wave can always be an incident plane wave behind the shock wave, whose wave angle is limited to

$$\theta_{if2} \in \begin{cases} [-\pi,\ -\pi + \beta_{n2}) \cup (\pi - \beta_{n2},\ \pi], & \text{when } M_2 < 1, \\ \{[-\pi,\ -\pi + \beta_{n2}) \cup (\pi - \beta_{n2},\ \pi]\} \cap (-\beta_{m2} - \beta_2,\ \pi + \beta_{m2} - \beta_2), & \text{when } M_2 > 1, \end{cases} \tag{2.46}$$

in which range one has

$$\alpha_q/\alpha_{if2} = (\cos\theta_{if2} + 1/M_{n2}) > 0, \quad \Delta_2/\alpha_{if2}^2 = (\cos\theta_{if2}/M_{n2} + 1)^2 \geqslant 0, \tag{2.47a,b}$$

Condition	θ_{if1}	θ_{ie1}	θ_{iv1}	θ_{is1}	θ_{if2}	θ_{ie2}	θ_{iv2}	θ_{is2}	θ_{f2}	θ_{e2}	θ_{v2}	θ_{s2}	θ_{d2}
Equations (2.42), (2.43*a*)	√	√	√	√					√	√	√	×	×
Equations (2.42), (2.43*b*)	√	√	√	√					×	√	√	√	×
Equations (2.42), (2.43*c*)	√	√	√	√					×	√	√	×	√
Equation (2.46)					√	×	×	×	√	√	√	×	×
Equation (2.48)					×	×	×	√	×	√	√	√	×

TABLE 2. Causal relationship between incident and excited waves, where subscript i indicates the incident wave, 1 (2) indicates whether the wave is before (after) the shock wave, and f, e, v, s, d represent fast acoustic, entropy, vorticity, slow acoustic and damped waves, respectively.

indicating that an incident fast acoustic wave behind the shock wave can only stimulate a fast acoustic wave and, of course, entropy and vorticity waves after the shock wave.

The slow acoustic wave can be an incident plane wave behind the shock wave only when $M_2 > 1$, and its wave angle is limited to

$$\theta_{is2} \in (-\beta_{n2}, \beta_{n2}) \cap (\beta_{m2} - \beta_2, \pi - \beta_{m2} - \beta_2), \quad \text{when } M_2 > 1, \tag{2.48}$$

in which range one has

$$\alpha_q/\alpha_{is2} = (\cos\theta_{is2} - 1/M_{n2}) < 0, \quad \Delta_2/\alpha_{is2}^2 = (\cos\theta_{is2}/M_{n2} - 1)^2 \geqslant 0, \tag{2.49a,b}$$

leading to the conclusion that an incident slow acoustic wave behind the shock wave can only excite a slow acoustic wave and, of course, entropy and vorticity waves after the shock wave.

Table 2 gives the causal relationship between the incident and excited waves, which clearly shows that four typical types of plane wave can be incident waves before the shock wave, but only fast and slow acoustic waves can be incident waves after the shock wave. The entropy–vorticity wave can always be stimulated after the shock wave, regardless of the type of incident wave. Fast and slow acoustic waves and damped waves can be excited by any type of typical plane wave before the shock wave, but they cannot coexist. When the incident plane wave is behind the shock wave, there is a phenomenon where the fast and slow acoustic waves can only be produced by themselves.

2.5. *Amplitude relationship of a plane wave across an oblique shock wave*

When non-dimensionalized, equation (2.15) governing the disturbances across an oblique shock wave can be rewritten as

$$\boldsymbol{B}\boldsymbol{U}_1'|_{x_s=0} = \boldsymbol{U}_2'|_{x_s=0} + \boldsymbol{C}_b u_d'|_{x_s=0}, \tag{2.50}$$

where $\boldsymbol{U}_1'$ is the disturbance before the shock wave, while $\boldsymbol{U}_2'$ is the disturbance after it, and we put

$$u_d' = u_d'^*/u_{02}^*, \quad \boldsymbol{B} = \boldsymbol{A}_2^{-1}\boldsymbol{L}_2^{*-1}\boldsymbol{L}_1^*\boldsymbol{A}_1, \quad \boldsymbol{C}_b = (\boldsymbol{B}\boldsymbol{R}_1^*\boldsymbol{C}_{b1}^* - \boldsymbol{R}_2^*\boldsymbol{C}_{b2}^*)u_{02}^*, \quad \boldsymbol{A}^* = \boldsymbol{L}^*\boldsymbol{A}\boldsymbol{R}^*. \tag{2.51a–d}$$

The components of the pre-shock disturbance ($\boldsymbol{U}_1'$) are very simple. According to table 2, they can be a fast acoustic wave, entropy wave, vorticity wave and slow acoustic wave and all are incident waves. Although these four plane waves may have different phases Θ, we can suppose that they have the same phases Ψ at $x_s = 0$. So, the pre-shock disturbance ($\boldsymbol{U}_1'$) can be written in a matrix form without losing generality:

$$\boldsymbol{U}_1'|_{x_s=0} = (\boldsymbol{C}_{if1}\hat{a}_{if1} + \boldsymbol{C}_{ie1}\hat{a}_{ie1} + \boldsymbol{C}_{iv1}\hat{a}_{iv1} + \boldsymbol{C}_{is1}\hat{a}_{is1})\exp(\mathrm{i}\Psi_1) + \text{c.c.}, \tag{2.52}$$

where $\boldsymbol{C}$ is one of the eigenvectors in (2.23) and $\hat{a}$ is the corresponding amplitude.

The components of the post-shock disturbance ($\boldsymbol{U}_2'$) are complicated. According to table 2, fast and slow acoustic waves can be incident plane waves after the shock wave, and an entropy–vorticity wave can always be excited behind the shock wave; however, only one of the fast acoustic wave, slow acoustic wave or damped wave can be stimulated by a given incident plane wave. Equation (2.29) implies that the frequency ω_2 and wavenumber α_{y2} of any type of wave excited by an incident plane wave are the same and are related to those of the incident wave, such that the disturbances before and after the shock wave have the same phases Ψ at $x_s = 0$. So we can generally combine the waves behind the shock into the post-shock disturbance ($\boldsymbol{U}_2'$) in a matrix form at $x_s = 0$, as per

$$\boldsymbol{U}_2'|_{x_s=0} = (\boldsymbol{C}_{c2}\hat{a}_{c2} + \boldsymbol{C}_{e2}\hat{a}_{e2} + \boldsymbol{C}_{v2}\hat{a}_{v2} + \boldsymbol{C}_{if2}\hat{a}_{if2} + \boldsymbol{C}_{is2}\hat{a}_{is2})\exp(\mathrm{i}\Psi_2) + \text{c.c.}, \tag{2.53}$$

where $\boldsymbol{C}_{c2}$ is one of $\boldsymbol{C}_{f2}$, $\boldsymbol{C}_{s2}$ and $\boldsymbol{C}_{d2}$, and the determination is based on the condition in (2.41) in which the universal wavenumbers α_q and α_p are determined by the incident wave in (2.30).

On the one hand, there are six incident waves in the disturbances $\boldsymbol{U}_1'$ and $\boldsymbol{U}_2'$, namely, $\boldsymbol{C}_{if1}$, $\boldsymbol{C}_{ie1}$, $\boldsymbol{C}_{iv1}$, $\boldsymbol{C}_{is1}$, $\boldsymbol{C}_{if2}$ and $\boldsymbol{C}_{is2}$, whose amplitudes $\hat{a}_{if1}$, $\hat{a}_{ie1}$, $\hat{a}_{iv1}$, $\hat{a}_{is1}$, $\hat{a}_{if2}$ and $\hat{a}_{is2}$ are known or are given as one input parameter of the incident wave. One can only set one of their amplitudes to be non-zero to investigate the interaction between that wave and the shock wave.

On the other hand, there are three excited waves in the post-shock disturbance $\boldsymbol{U}_2'$, namely, $\boldsymbol{C}_{c2}$, $\boldsymbol{C}_{e2}$ and $\boldsymbol{C}_{v2}$, whose amplitudes $\hat{a}_{c2}$, $\hat{a}_{e2}$ and $\hat{a}_{v2}$ are unknown. Another unknown parameter is the velocity of the distorted shock wave in the x direction, namely, $\hat{u}_d$. Those four unknown parameters can be solved by substituting (2.52) and (2.53) into (2.50), as follows:

$$[\hat{a}_{c2}, \hat{a}_{e2}, \hat{a}_{v2}, \hat{u}_d]^{\mathrm{T}} = \boldsymbol{D}_{if1}\hat{a}_{if1} + \boldsymbol{D}_{ie1}\hat{a}_{ie1} + \boldsymbol{D}_{iv1}\hat{a}_{iv1} + \boldsymbol{D}_{is1}\hat{a}_{is1} - \boldsymbol{D}_{if2}\hat{a}_{if2} - \boldsymbol{D}_{is2}\hat{a}_{is2}, \tag{2.54}$$

where

$$\boldsymbol{E}_{c2}^{-1} = [\boldsymbol{C}_{c2}, \boldsymbol{C}_{e2}, \boldsymbol{C}_{v2}, \boldsymbol{C}_b], \quad \boldsymbol{D}_{i1} = \boldsymbol{E}_{c2}\boldsymbol{B}\boldsymbol{C}_{i1}, \quad \boldsymbol{D}_{i2} = \boldsymbol{E}_{c2}\boldsymbol{C}_{if2}. \tag{2.55a–c}$$

2.6. *Transmission, reflection and generation coefficients*

The transmission or reflection coefficient is defined as the ratio of an amplitude quantity in the transmitted or reflected disturbance wave to the corresponding quantity in the incident wave, namely,

$$T_f \equiv \frac{\hat{p}_2'^*}{\hat{p}_{if1}'^*} = u_b\frac{\hat{a}_{f2} + \hat{a}_{s2} + \hat{a}_{d2}}{\hat{a}_{if1}} = T_{ff} + T_{fs} + T_{fd}, \quad R_f \equiv \frac{\hat{p}_2'^*}{\hat{p}_{if2}'^*} = \frac{\hat{a}_{f2}}{\hat{a}_{if2}}, \tag{2.56a,b}$$

$$T_s \equiv \frac{\hat{p}_2'^*}{\hat{p}_{is1}'^*} = u_b \frac{\hat{a}_{f2} + \hat{a}_{s2} + \hat{a}_{d2}}{\hat{a}_{is1}} = T_{sf} + T_{ss} + T_{sd}, \quad R_s \equiv \frac{\hat{p}_2'^*}{\hat{p}_{is2}'^*} = \frac{\hat{a}_{s2}}{\hat{a}_{is2}}, \tag{2.56c,d}$$

$$T_e \equiv \frac{\hat{\rho}_2'^*}{\hat{\rho}_{ie1}'^*} = \frac{\hat{a}_{e2} + M_{n2}^2(\hat{a}_{f2} + \hat{a}_{s2} + \hat{a}_{d2})}{u_b \hat{a}_{ie1}} = T_{ee} + T_{ef} + T_{es} + T_{ed}, \tag{2.56e}$$

$$T_v \equiv \frac{\sqrt{\hat{u}_2'^{*2} + \hat{v}_2'^{*2}}}{\sqrt{\hat{u}_{iv1}'^{*2} + \hat{v}_{iv1}'^{*2}}} = u_b \frac{\sqrt{(X_1)^2 + (X_2)^2}}{\hat{a}_{iv1}}, \tag{2.56f}$$

$$T_{vv} \equiv \frac{\sqrt{\hat{u}_{v2}'^{*2} + \hat{v}_{v2}'^{*2}}}{\sqrt{\hat{u}_{iv1}'^{*2} + \hat{v}_{iv1}'^{*2}}} = u_b \frac{|\hat{a}_{v2}|}{\hat{a}_{iv1}}, \quad T_{vc} \equiv \frac{\sqrt{\hat{u}_{c2}'^{*2} + \hat{v}_{c2}'^{*2}}}{\sqrt{\hat{u}_{iv1}'^{*2} + \hat{v}_{iv1}'^{*2}}} = u_b \frac{M_{n2}|\hat{a}_{c2}|}{\hat{a}_{iv1}}, \tag{2.56g,h}$$

in which the contributions of each excited wave to the incident wave are also defined to evaluate their importance; c represents one of f, s and d, and $X_1 = M_{n2}(\cos\theta_{f2}\,\hat{a}_{f2} - \cos\theta_{s2}\,\hat{a}_{s2} - g_{x2}\hat{a}_{d2}) - \sin\theta_{v2}\,\hat{a}_{v2}$, $X_2 = M_{n2}(\sin\theta_{f2}\,\hat{a}_{f2} - \sin\theta_{s2}\,\hat{a}_{s2} - g_{y2}\hat{a}_{d2}) - \cos\theta_{v2}\,\hat{a}_{v2}$.

A generation coefficient is the ratio of a quantity in a generated wave to the quantity of the same dimension in the incident disturbance wave. The generation coefficients for the pressure fluctuation behind the shock wave corresponding to the incident entropy and vorticity waves are defined as

$$G_e \equiv -\frac{\hat{p}_2'^*/p_{01}^*}{\hat{\rho}_{ie1}'^*/\rho_{01}^*} = -u_b \gamma M_{n1}^2 \frac{\hat{a}_{f2} + \hat{a}_{s2} + \hat{a}_{d2}}{\hat{a}_{ie1}} = G_{ef} + G_{es} + G_{ed}, \tag{2.57a}$$

$$G_v \equiv \frac{\hat{p}_2'^*/p_{01}^*}{\sqrt{\hat{u}_{iv1}'^{*2} + \hat{v}_{iv1}'^{*2}}/c_{01}^*} = u_b \gamma M_{n1} \frac{\hat{a}_{f2} + \hat{a}_{s2} + \hat{a}_{d2}}{\hat{a}_{iv1}} = G_{vf} + G_{vs} + G_{vd}. \tag{2.57b}$$

3. Verification

3.1. *Theoretical verification*

In order to validate the correctness and accuracy of our theoretical approach, the results of T_f, G_v, G_e and R_f, as functions of the incident wave angle θ_i for three different shock wave angles β_1 with $M_1 = 8$ and $\gamma = 5/3$, are shown in figure 2, in which the theoretical solutions of McKenzie & Westphal (1968) are also provided for comparison. Good agreement between our results and the theoretical solutions can be seen within most of the range of θ_i, except when a damped wave is excited. This case was not considered by McKenzie & Westphal (1968), indicating that our approach is a further improvement of the theory. It is also worth mentioning that in figure 2(*d*), there is a certain range of θ_{if2} within which our result is absent but the theoretical solution is present, because this solution does not satisfy the condition of $\omega > 0$.

3.2. *Numerical verification*

For the case of a normal shock wave, we performed DNS to verify our theoretical results. The governing equation is a one-dimensional unsteady compressible Euler equation in conservative form, derived from a calorically and thermally perfect gas model. Uniform grids are used in the streamwise direction and the number of grid points per wavelength is greater than 50. The convective term is discretized by employing the fifth-order WENO scheme with Lax–Friedrichs (LF) flux splitting,

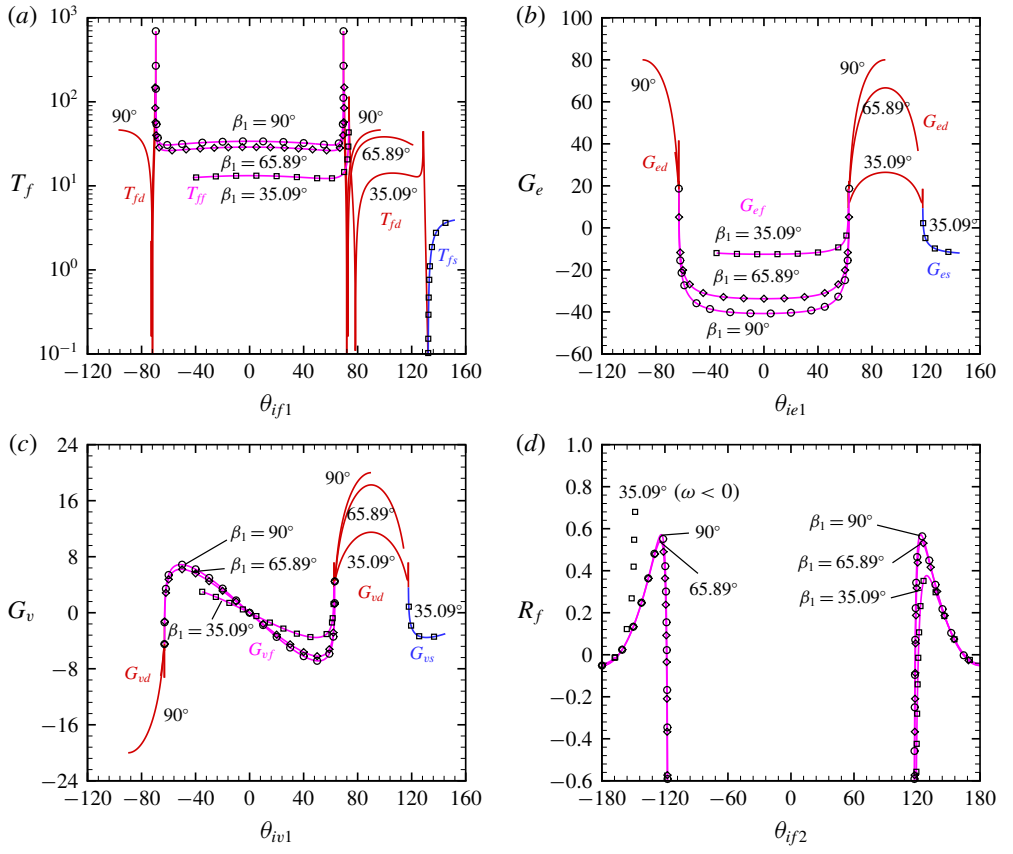

FIGURE 2. (Colour online) Comparison of the coefficients of our results (lines) and the theoretical solutions (symbols; McKenzie & Westphal 1968) for three shock wave angles β_1 with $M_1 = 8$ and $\gamma = 5/3$: (*a*) T_f for incident fast acoustic waves; (*b*) G_e for incident entropy waves; (*c*) G_v for incident vorticity waves; and (*d*) R_f for incident fast acoustic waves. The value $\beta_1 = 90°$ (○) corresponds to a normal shock wave; $\beta_1 = 65.89°$ (◇) corresponds to an oblique shock wave with subsonic flow behind; and $\beta_1 = 35.09°$ (□) corresponds to an oblique shock wave with supersonic flow behind.

while the third-order Runge–Kutta (RK) method is used for temporal evolution. An incident wave is introduced continuously at the inlet, while a non-reflecting boundary condition is applied at the outlet. For the case of an oblique shock wave, we used the DNS result presented by Su & Geng (2017). Figure 3 compares our theoretical results with the DNS results, demonstrating good agreement for cases of both normal and oblique shock waves.

4. Analysis and results

4.1. *Physical essence of damped waves*

According to (2.18), one can obtain the dispersion relationship in the real number space only for acoustic waves:

$$(\alpha_x + v_0\alpha_y - \omega)^2 - (\alpha_x^2 + \alpha_y^2)/M_n^2 = 0, \tag{4.1}$$

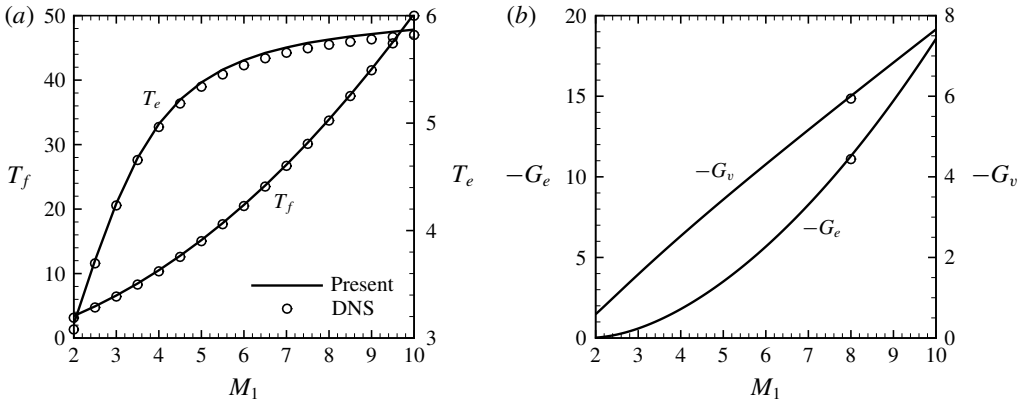

FIGURE 3. Comparison of the coefficients of our results and the DNS results: (*a*) T_f and T_e for a normal shock wave with $\beta_1 = 90°$, incident wave angle $\theta_{i1} = 0°$ and $\gamma = 1.4$, with the DNS performed by us; and (*b*) G_e and G_v for an oblique shock wave with $\beta_1 = 35.09°$ and $\beta_1 = 65.89°$, respectively, incident wave angle $\theta_{i1} = 45°$ and $\gamma = 5/3$, with the DNS result given by Su & Geng (2017).

whose condition of solvability with respect to α_x in the real number space is

$$\Delta = \frac{4}{M_n^2}\left[(v_0\alpha_y - \omega)^2 + \left(1 - \frac{1}{M_n^2}\right)\alpha_y^2\right] \geqslant 0. \tag{4.2}$$

For pre-shock flow with a normal Mach number significantly greater than one ($M_{n1} > 1$), the condition of solvability is established without any preconditions, implying that the fast and slow acoustic waves always exist before the shock wave. However, for post-shock flow where $M_{n2} < 1$, the above condition of solvability is not always true any more, indicating that there is a certain region when there are no solutions for the fast and slow acoustic waves. In order to perfect the solution of the dispersion relation, we extend the form of the solution from the real number space to the complex number space by introducing a new real parameter in the normal mode of disturbance. We thereby obtain an additional solution, namely, a damped wave. It is easy to prove that, when the above condition of solvability does not hold, it is equivalent to (2.22). Because the damped wave is also a solution of the dispersion relationship for acoustic waves, and its eigenvector $\boldsymbol{C}_d$ in (2.23) is very similar to those of $\boldsymbol{C}_f$ and $\boldsymbol{C}_s$, it can be regarded as a special acoustic solution.

Figure 4 depicts cross-sections of the wave normal surface of plane waves in terms of polar coordinates (α, θ) for supersonic flow ($M_n > 1$) and subsonic flow ($M_n < 1$). It can be seen that the wave normal surface of an entropy–vorticity wave with a given frequency forms a straight line (green line with circles), whose direction is perpendicular to the flow direction, regardless of the base flow being supersonic or subsonic. Meanwhile the wave normal surface of an acoustics wave depends on the base flow condition.

When the base flow is supersonic, as shown in figure 4(*a*), the wave normal surfaces of fast and slow acoustic waves manifest as a hyperbola, whose axis is parallel to the flow direction and whose asymptotes deviate from the flow direction at an angle $\beta_m = \arcsin(1/M)$. The branch of the hyperbola close to the coordinate origin (purple line with downward-pointing triangles) corresponds to the fast acoustic wave, while

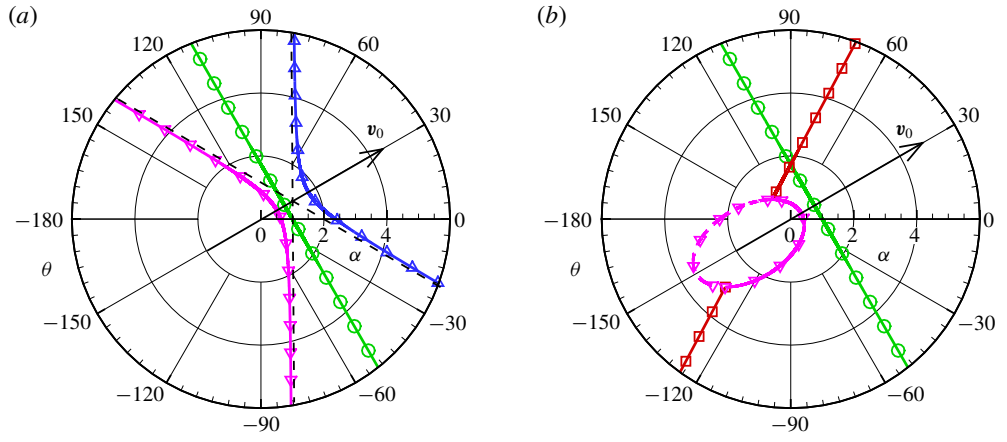

FIGURE 4. (Colour online) Cross-sections of the wave normal surface of plane waves in polar coordinates (α, θ) for (a) supersonic flow with $M = 2$, $\beta = 60°$, and (b) subsonic flow with $M = 0.8$, $\beta = 60°$. The green line with ○ represents the entropy–vorticity wave, the purple line with ▽ represents the fast acoustic wave, the blue line with △ represents the slow acoustic wave and the red line with □ represents the damped wave. The solid line indicates $u_{gx} \geqslant 0$, while the dashed line indicates $u_{gx} < 0$, where u_{gx} is the x component of the group velocity.

another branch (blue line with upward-pointing triangles) represents the slow acoustic wave.

When the base flow is subsonic, as shown in figure 4(b), the wave normal surface of a fast acoustic wave presents as an ellipse with its major axis pointing along the flow direction and its origin located at the forward focus. The ellipse can be divided into two parts according to the sign of the x component of group velocity. The dashed line indicates $u_{gx} < 0$ for a given positive frequency ω. Some people think this is a solution for a slow acoustic wave, because its frequency can be treated as a negative value $(-\omega)$. However, as mentioned in § 2.4.2, this would lead to ambiguity in the definition of a fast/slow acoustic wave. Based on the fundamental limitation of $\omega > 0$, the slow acoustic wave does not exist in the subsonic base flow; instead, a damped wave appears, whose wave normal surface presents as a straight line (red line with squares). The straight line of the damped wave is mutually cut by the ellipse of the fast acoustic wave at the junction of the solid and dashed lines.

Figure 5 depicts the distribution of the phase velocity and group velocity of the excited waves behind the shock wave in polar coordinates when $M_1 = 2$ and $\beta_1 = 60°$, respectively. It can be clearly seen that the damped wave plays a bridging role, as it connects the fast and slow acoustic waves at two special angles. The two special angles of the phase velocity are symmetrical with an axis $\theta = 90°$ and those of the group velocity are equal to $\theta = 90°$ when the angle of the incident wave reaches its critical angle, indicating that the essence of the critical angle is that the x component of the group velocity is zero.

4.2. *Contribution of each excited wave to the transmission coefficient*

Because the fast acoustic wave, slow acoustic wave and damped wave cannot be stimulated after the shock wave at the same time, the transition coefficients of the

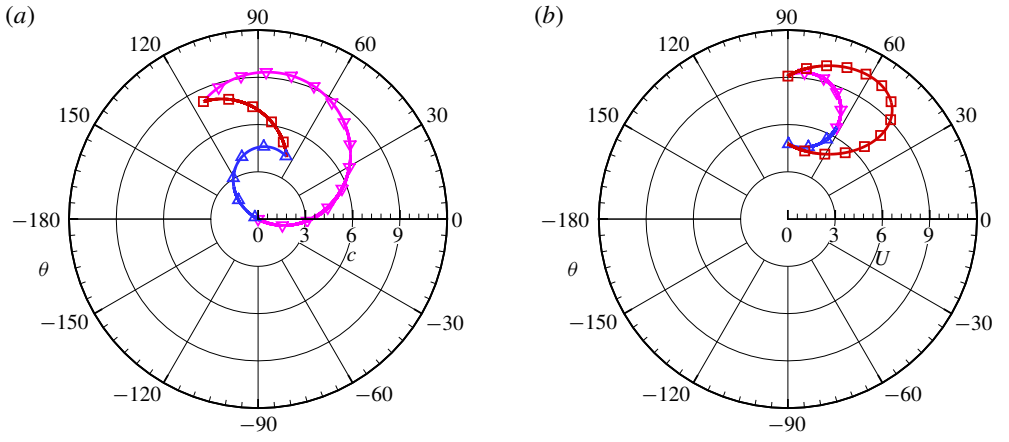

FIGURE 5. (Colour online) Distribution of (*a*) the phase velocity and (*b*) the group velocity of excited waves behind the shock wave in polar coordinates when $M_1 = 2$ and $\beta_1 = 60°$. The meanings of lines and symbols are the same as those in figure 4.

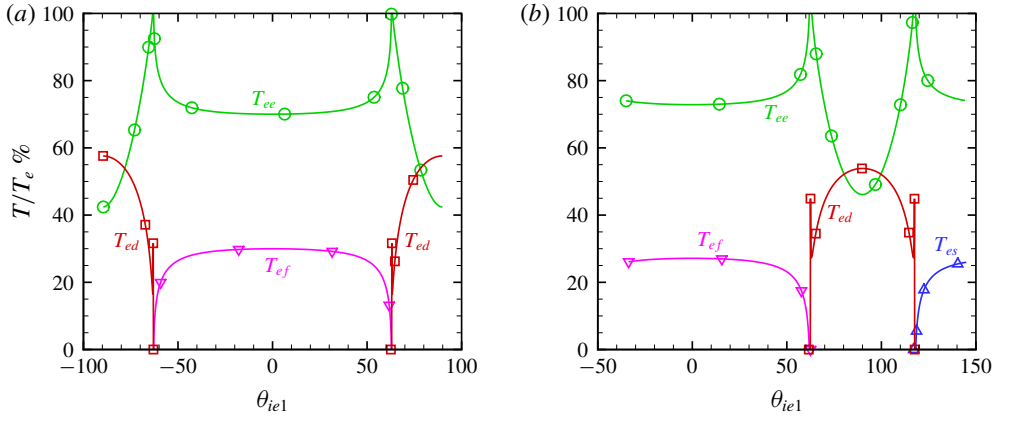

FIGURE 6. (Colour online) Contribution of each excited wave to the entropy wave transmission coefficient for post-shock base flows that are (*a*) subsonic ($M_2 < 1$ with $\beta_1 = 90°$) and (*b*) supersonic ($M_2 > 1$ but $M_{n2} < 1$ with $\beta_1 = 35.09°$). The pre-shock base flow satisfies $M_1 = 8$ and $\gamma = 5/3$. The lines and symbols represent the same parameters as in figure 4.

fast acoustic wave T_f and slow acoustic wave T_f are only provided by one of the excited waves in (2.56); however, the transition coefficients of the entropy wave T_e and vorticity wave T_v are always provided by two excited waves. So, it is necessary to evaluate the contribution of each excited wave to the transmission coefficient.

Figure 6 shows the contribution of each excited wave to the entropy wave transmission coefficient. It can be seen that T_{ee} contributes approximately 70 % and T_{ef} or T_{es} contributes almost 30 % to T_e in most of the entropy wave's incident angle range, regardless of the post-shock base flow being subsonic or supersonic. This indicates that both the excited entropy wave and excited fast/slow waves have equivalent importance. When the incident angle is close to the critical angle, T_e is

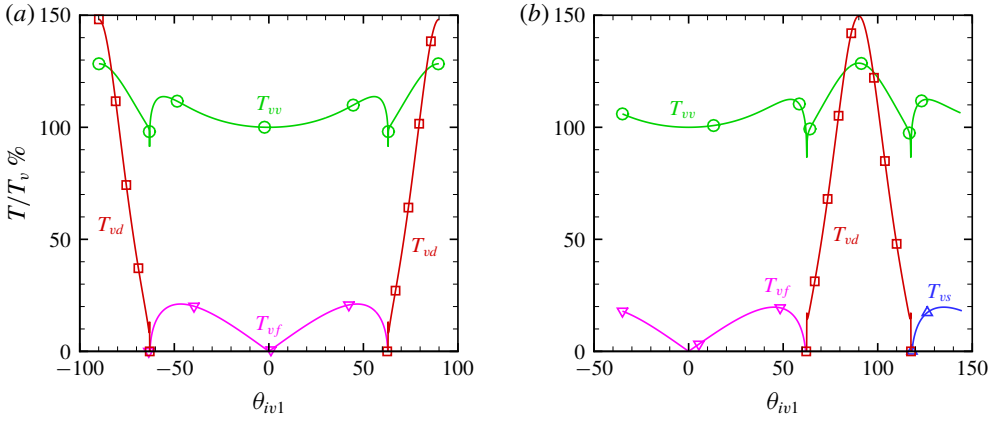

FIGURE 7. (Colour online) Contribution of each excited wave to the vorticity wave transmission coefficient when the post-shock base flow is (*a*) subsonic ($M_2 < 1$ with $\beta_1 = 90°$) and (*b*) supersonic ($M_2 > 1$ but $M_{n2} < 1$ with $\beta_1 = 35.09°$). The pre-shock base flow satisfies $M_1 = 8$ and $\gamma = 5/3$. The lines and symbols are the same as those in figure 4.

mainly contributed to by T_{ee}, while the contributions of T_{ef}, T_{es} and T_{ed} are zero. When the damped wave is excited, its contribution to T_e increases and reaches a maximum value of approximately 60 %, while the contribution of T_{ee} decreases and reaches a minimum value of approximately 40 %. Because the amplitude of the damped wave will decay, the amplitude of the disturbance behind and far away from the shock wave will significantly decrease at a certain incident wave angle when the damped wave is stimulated.

Figure 7 depicts the contribution of each excited wave to the vorticity wave transmission coefficient. It can be seen that T_{vv} makes an approximately 110 % contribution to T_v, while T_{vf} or T_{vs} contribute less than 20 % in most of the vorticity wave's incident angle range for all kinds of post-shock base flow, indicating that the excited fast/slow wave is not important to the amplitude of the post-shock disturbance. Unlike the incident entropy wave, for the incident vorticity wave, the amplitude of the disturbance behind and far away from the shock wave is increased by approximately 20 % when the damped wave is stimulated.

4.3. *Distribution of the transmission coefficient in the M_1–θ_i plane*

Figure 8 shows the contours of the transmission coefficient for each type of incident plane wave in the M_1–θ_i plane under the conditions of $\beta_1 = 90°$ and $\beta_1 = 35.09°$, respectively. From this, it can be seen that the incident wave angle θ_i is divided into five regions. The angles in the bottom and top regions are beyond the angle limitation of the incident plane wave, leading to all of the transmission coefficients being zero. The angles in the middle are split into three parts by two critical angles, which are governed by (2.43). In the case of $\beta_1 = 90°$, when the post-shock base flow is subsonic, the excited waves for the incident angles in these three parts are a damped wave, fast acoustic wave and damped wave, successively. Meanwhile, in the case of $\beta_1 = 35.09°$, when the post-shock base flow is supersonic, the excited waves are a fast acoustic wave, damped wave and slow acoustic wave. In these three parts, the incident wave

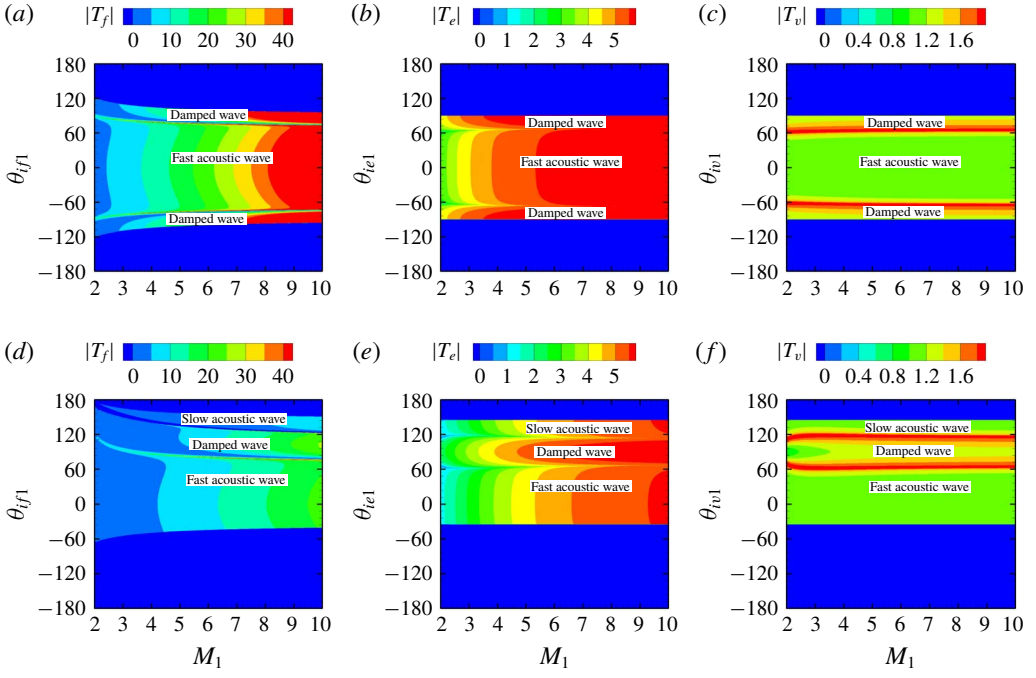

FIGURE 8. (Colour online) Contours of (*a*) $|T_f|$, (*b*) $|T_e|$ and (*c*) $|T_v|$ in the M_1–θ_i plane ($\gamma = 1.4$). Panels (*a–c*) show the results of a normal shock wave with $\beta_1 = 90°$ for a subsonic post-shock base flow. Panels (*d–f*) show the results of an oblique shock wave with $\beta_1 = 35.09°$ for a supersonic post-shock base flow.

angle required to excite the fast acoustic wave occupies most of the angle range. The fast acoustic transmission coefficient is relatively unaffected by the incident wave angle, while the other two coefficients are more dependent on it. The transmission coefficients near the critical angles are abnormal, being too small or too large, which may be caused by the asymptotic property of the theoretical method.

In figure 8(*a–c*), for a normal shock wave with $\beta_1 = 90°$, the transmission coefficient is symmetric with respect to the axis of $\theta_1 = 0$. The transmission coefficients for the fast acoustic wave and entropy wave increase with increases in the free-stream Mach number M_1, while this number has little effect on the vorticity wave transmission coefficient. For most of the range of the free-stream Mach number, $|T_f|$ and $|T_e|$ are greater than 1, especially $|T_f|$, which is almost one order of magnitude higher than $|T_e|$, implying that the amplitude of the pressure and density disturbance will always be magnified after passing through the shock wave. And T_v is approximately 1 in the whole M_1–θ_i plane, except for the region near the critical angles, indicating that there is no significant amplification or attenuation of the velocity disturbance amplitude behind the shock wave.

Figure 8(*d–f*) shows that, for an oblique shock wave with $\beta_1 = 35.09°$, the symmetry of the transmission coefficient is destroyed and the non-zero region deflects to the positive side of the incident wave angle. Because the post-shock base flow is supersonic, a slow acoustic wave can be excited and its region is connected to that of a fast acoustic wave by a damped wave region. Compared with the case of $\beta_1 = 90°$,

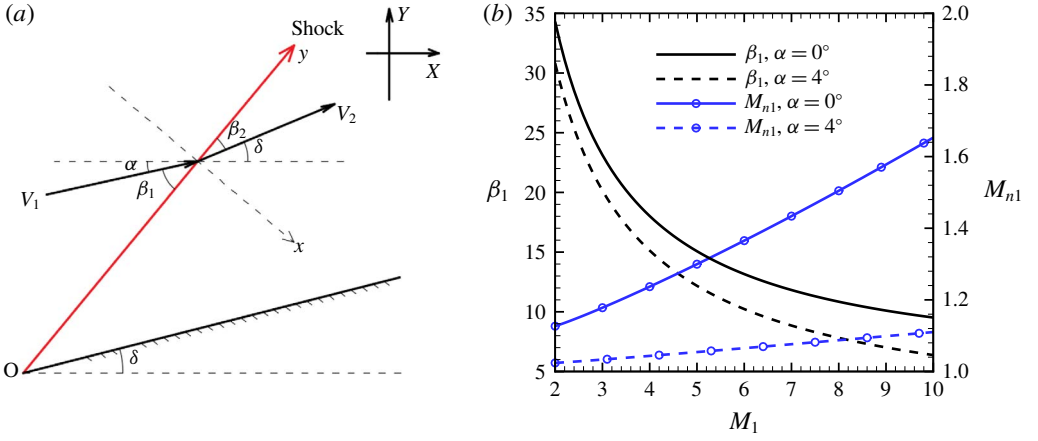

FIGURE 9. (Colour online) (*a*) Physical model of a wedge and (*b*) dependence of shock wave angle β_1 and normal Mach number M_{n1} on free-stream Mach number M_1 for two angles of attack α.

the transmission coefficient in the case of $\beta_1 = 35.09°$ is much smaller, illustrating that the inclination of an oblique shock wave can lead to a reduction in the transmission coefficient.

4.4. *Engineering application to a wedge model*

For a two-dimensional sharp wedge model with a specific semi-angle δ, as shown in figure 9(*a*), the relationship between the shock wave angle β_1 and the free-stream Mach number M_1 for a given angle of attack α can be described by the following equation:

$$\tan(\delta - \alpha) = 2\cot\beta_1 \frac{M_1^2 \sin^2\beta_1 - 1}{M_1^2[\gamma + \cos(2\beta_1)] + 2}. \tag{4.3}$$

By solving this, we can express the values of β_1 as a function of M_1 for two angles of attack when $\delta = 5°$, and the results are shown in figure 9(*b*), in which the corresponding normal Mach number before the shock wave is also given. It can be seen that the shock wave angle β_1 rapidly decreases with the increase of the free-stream Mach number, while the normal Mach number increases slowly. The greater the angle of attack, the faster the shock wave angle decreases and the slower the normal Mach number increases.

Figure 10 shows the contours of the transmission coefficient for three types of incident plane wave in the M_1–ϕ_i plane on a wedge model with a semi-angle $\delta = 5°$ for two angles of attack. Here the incident angle $\phi_i = \theta_i + \beta_1 + \delta - \pi/2$ is defined as the angle between the wavevector direction and the horizontal direction. As mentioned in the above section, the inclination of an oblique shock wave can lead to a reduction in the transmission coefficient. The transmission coefficients in figure 10 are much smaller than those in figure 8, because most of the shock wave angles of the former are much smaller than those of the latter. Furthermore, the transmission coefficients in figure 10(*d–f*) when $\alpha = 4°$ are smaller than those in figure 10(*a–c*) when $\alpha = 0°$, because the angle of attack can decrease the shock wave angle β_1, as can be seen in

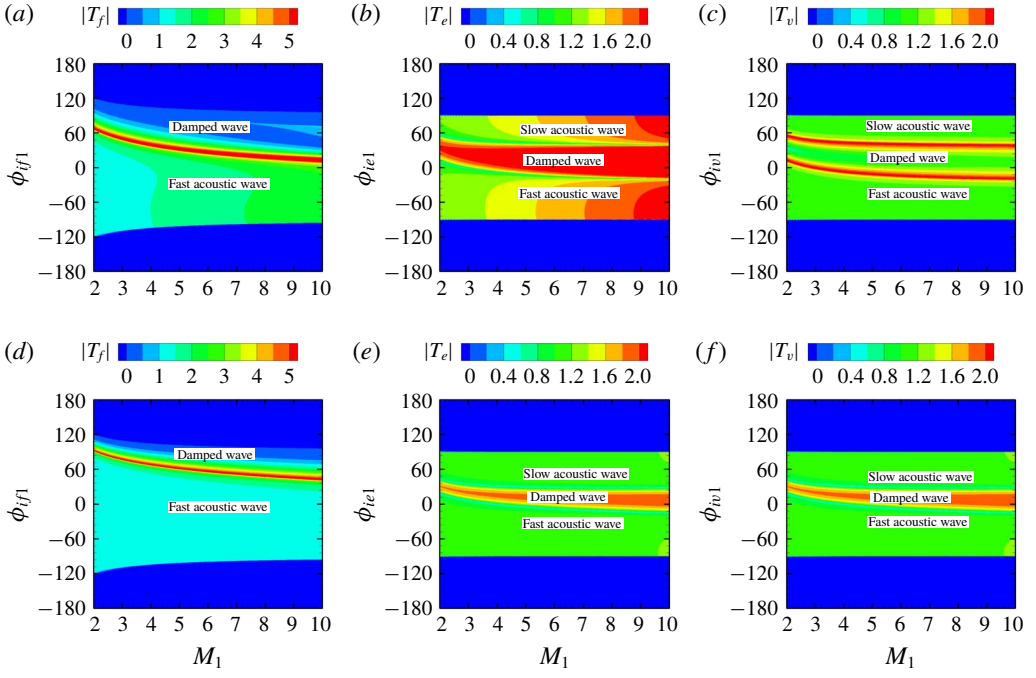

FIGURE 10. (Colour online) Contours of (*a*) $|T_f|$, (*b*) $|T_e|$ and (*c*) $|T_v|$ in the M_1–ϕ_i plane on a wedge model with semi-angle $\delta = 5°$. Panels (*a–c*) are the case of $\alpha = 0°$, while panels (*d–f*) are for the case of $\alpha = 4°$. The incident angle $\phi_i = \theta_i + \beta_1 + \delta - \pi/2$ is the angle between the wavevector direction and the horizontal direction.

figure 9(*b*). The regions of a damped wave in figure 10(*d–f*) are much narrower than those in figure 10(*a–c*), indicating that the angle of attack can reduce the incident angle ϕ_i required to excite a damped wave. Most of the transmission coefficients for the three types of incident plane wave on the wedge model are approximately 1, implying that the amplitude of the post-shock disturbances is of the same order as that before the shock wave. So, the incident disturbance can be treated as passing through the shock wave directly without considering its amplitude amplification.

5. Summary and conclusions

In the present paper, we investigated the interaction between disturbances and an oblique shock wave, focusing on what happens when no post-shock acoustic waves are generated.

The interaction between disturbances and shock waves has usually been solved by a theoretical approach, called linear interaction analysis (LIA). The disturbances before and after the shock wave are governed by the linearized Euler equation, while the discontinuity of base flow and disturbance is dealt with by the Rankine–Hugoniot condition. The dispersion relationship was solved in a real number space, leading to four typical types of plane wave, namely, fast acoustic, entropy, vorticity and slow acoustic waves.

Unlike the classical LIA, a new real parameter to describe the decay in amplitude was introduced and the dispersion relationship was solved in a complex number

space. Additionally, the concept of a damped wave was proposed, which is a type of excited plane wave whose eigenvector is similar to those of fast and slow acoustic waves. Two universal kinds of wavenumber for the excited wave were defined to study conveniently: (1) α_q, the equivalent wavenumber perpendicular to the shock surface; and (2) α_p, the wavenumber parallel to it. The dispersion relationship between any incident plane wave and post-shock excited waves was constructed analytically. The angle limitations of the base flow, plane wave and incident plane wave were discussed. There are two critical angles that excite fast and slow acoustic waves, between which the incident angle can be divided into three regions. In each region, only one of the fast and slow acoustic waves and damped wave can be excited, implying that these three types of plane wave cannot be stimulated at the same time by any single incident wave. However, there are no angle limitations on the excitation of entropy and vorticity waves. The causal relationships between incident and excited waves were demonstrated. There are six types of incident wave, four pre-shock and post-shock, while there are only three types of plane wave that can be excited at the same time by any single incident wave. By considering distortion in the shock wave and its velocity in the x direction, the amplitude relationship between the six incident waves and three excited waves was established analytically, systematically and comprehensively.

Our theoretical approach was validated and verified using the theoretical solution of McKenzie & Westphal (1968) and DNS. Good agreement was found in all comparisons, indicating that our approach is a further improvement of the LIA theory and method.

The physical essence of damped waves was discussed. The condition of solvability of the dispersion relationship in a real number space always holds for pre-shock base flow, but not for post-shock base flow under certain conditions, leading to the dispersion relationship solution requiring a complex number space. The damped wave solution is done in the complex number space, with an imaginary component representing the decay in amplitude. Cross-sections of the normal surface of each wave were shown, through which wave parameter behaviour was discussed in terms of polar coordinates. The wave normal surface of a damped wave presents as a straight line and is mutually cut by the wave normal surface (an ellipse) of a fast acoustic wave. The distributions of phase velocity and group velocity show that damped waves play a bridging role by connecting fast and slow acoustic waves at two special angles related to the critical incident angles. The essence of the critical angles is that the x component of the group velocity is zero.

The importance of excited waves was discussed by evaluating the contribution of each excited wave to the transmission coefficient. When the incident wave is an entropy wave, both the excited entropy wave and excited fast/slow acoustic waves have equivalent importance. Meanwhile, when the incident wave is a vorticity wave, the excited vorticity wave plays a dominant role and the excited fast/slow acoustic waves are unimportant to the amplitude of post-shock disturbance. When a damped wave is excited by an incident entropy wave, the amplitude of disturbance behind and far away from the shock wave is significantly reduced, but there is an obvious increase when a damped wave is excited by an incident vorticity wave.

The distribution of the transmission coefficient in the M_1–θ_i plane was analysed. The free-stream Mach number M_1 has a great influence on the transmission coefficients of incident fast acoustic and entropy waves, but little influence on that of incident vorticity waves. The incident wave angle θ_i has a weak impact on the transmission coefficient, and only when a fast acoustic wave is excited. The inclination of the

oblique shock wave can lead to a reduction in the transmission coefficient. The amplitudes of the pressure and density disturbances will always be magnified after passing through the shock wave, while there is no significant amplification or attenuation of the post-shock velocity disturbance amplitude when the incident wave is a vorticity wave.

An engineering application with a wedge model was performed. As the free-stream Mach number M_1 increases, the shock wave angle β_1 decreases rapidly. Because the amplitude of the post-shock fluctuations has the same order as that before the shock wave, the incident disturbances can be treated as passing through the shock wave directly without considering amplitude amplification. Increasing the angle of attack can decrease the shock wave angle and then the transmission coefficient.

Acknowledgements

This work was supported by the National Numerical Wind Tunnel (no. 2018-ZT1A03), the National Natural Science Foundation of China (nos 11672351 and 11732011), the National Key Research and Development Program of China (no. 2016YFA0401200) and the Open Fund from State Key Laboratory of Aerodynamics (no. SKLA201601). The authors would also like to thank Professor J. Luo of Tianjin University for valuable discussions and suggestions.

Appendix A. Matrices and vectors

$$\boldsymbol{A}^* = \frac{\mathrm{d}\boldsymbol{E}^*}{\mathrm{d}\boldsymbol{U}^*} = \begin{bmatrix} u_0^* & \rho_0^* & 0 & 0 \\ u_0^* u_0^* & 2\rho_0^* u_0^* & 0 & 1 \\ u_0^* v_0^* & \rho_0^* v_0^* & \rho_0^* u_0^* & 0 \\ u_0^* e_0^* & \rho_0^*(u_0^{*2} + h_0^*) & \rho_0^* u_0^* v_0^* & \dfrac{\gamma}{\gamma - 1} u_0^* \end{bmatrix}, \quad \boldsymbol{C}_b^* = \begin{bmatrix} 0 \\ 1 - \dfrac{v_0^* \alpha_y^*}{\omega^*} \\ \dfrac{u_0^* \alpha_y^*}{\omega^*} \\ 0 \end{bmatrix}, \tag{A 1a,b}$$

where $e_0^* = (u_0^{*2} + v_0^{*2})/2$ is the kinetic energy and $h_0^* = e_0^* + (\gamma p_0^*/(\gamma - 1))/\rho_0^*$ is the total enthalpy;

$$\left.\begin{aligned} \boldsymbol{L}^* &= \rho_0^* u_0^* \begin{bmatrix} 1 & 0 & 0 & 0 \\ 0 & u_0^* & 0 & 0 \\ 0 & 0 & u_0^* & 0 \\ 0 & 0 & 0 & u_0^{*2} \end{bmatrix}, \quad \boldsymbol{R}^* = \frac{1}{\rho_0^* u_0^*} \begin{bmatrix} u_0^* & 0 & 0 & 0 \\ 0 & \rho_0^* & 0 & 0 \\ 0 & 0 & \rho_0^* & 0 \\ 0 & 0 & 0 & \dfrac{1}{u_0^*} \end{bmatrix}, \\ \boldsymbol{A} &= \begin{bmatrix} 1 & 1 & 0 & 0 \\ 1 & 2 & 0 & 1 \\ v_0 & v_0 & 1 & 0 \\ e_0 & 1 + h_0 & v_0 & \dfrac{\gamma}{\gamma - 1} \end{bmatrix}, \end{aligned}\right\} \tag{A 2}$$

$$\left.\begin{aligned}\boldsymbol{B} &= \begin{bmatrix} 2u_b - \dfrac{\gamma-1}{\gamma+1} & 2u_b - 2\dfrac{\gamma-1}{\gamma+1} & 0 & -\dfrac{2\gamma}{\gamma+1} \\ \dfrac{\gamma-1}{\gamma+1} - u_b & 2\dfrac{\gamma-1}{\gamma+1} - u_b & 0 & \dfrac{2\gamma}{\gamma+1} \\ 0 & 0 & 1 & 0 \\ \dfrac{2}{\gamma+1} & \dfrac{4}{\gamma+1} & 0 & -\dfrac{\gamma-1}{\gamma+1} \end{bmatrix}, \\ \boldsymbol{C}_d &= \begin{bmatrix} b_1 \\ b_2 \\ b_3 \\ b_4 \end{bmatrix} = \begin{bmatrix} 2\left(u_b - \dfrac{\gamma-1}{\gamma+1}\right)\dfrac{u_b\alpha_q}{\omega_1} \\ \left(\dfrac{\gamma-3}{\gamma+1} - u_b\right)\dfrac{u_b\alpha_q}{\omega_1} \\ (1-u_b)\dfrac{\alpha_p}{\omega_1} \\ \dfrac{4}{\gamma+1}\dfrac{u_b\alpha_q}{\omega_1} \end{bmatrix}, \end{aligned}\right\} \tag{A 3}$$

$$\boldsymbol{E}_{c2} = m \begin{bmatrix} 0 & -\cos\theta_{v2}\dfrac{b_4}{d_4} & -\sin\theta_{v2}\dfrac{b_4}{d_4} & \sin\theta_{v2}\dfrac{b_3}{d_4} + \cos\theta_{v2}\dfrac{b_2}{d_4} \\ \dfrac{1}{m} & \cos\theta_{v2}\dfrac{b_4d_1 - b_1d_4}{d_4} & \sin\theta_{v2}\dfrac{b_4d_1 - b_1d_4}{d_4} & \sin\theta_{v2}\dfrac{b_1d_3 - b_3d_1}{d_4} + \cos\theta_{v2}\dfrac{b_1d_2 - b_2d_1}{d_4} \\ 0 & -\dfrac{b_3d_4 - b_4d_3}{d_4} & \dfrac{b_2d_4 - b_4d_2}{d_4} & \dfrac{b_3d_2 - b_2d_3}{d_4} \\ 0 & \cos\theta_{v2} & \sin\theta_{v2} & -\sin\theta_{v2}\dfrac{d_3}{d_4} - \cos\theta_{v2}\dfrac{d_2}{d_4} \end{bmatrix}, \tag{A 4}$$

where $1/m = \sin\theta_{v2}(b_3d_4 - b_4d_3)/d_4 + \cos\theta_{v2}(b_2d_4 - b_4d_2)/d_4$; and $\boldsymbol{C}_{c2} = [d_1, d_2, d_3, d_4]^{\mathrm{T}}$ is one of $\boldsymbol{C}_{f2}$, $\boldsymbol{C}_{s2}$ or $\boldsymbol{C}_{d2}$.

REFERENCES

ARNAL, D. & CASALIS, G. 2000 Laminar–turbulent transition prediction in three-dimensional flows. *Prog. Aerosp. Sci.* **36** (2), 173–191.

D'IAKOV, S. P. 1958*a* Interaction of shock waves with small perturbations I. *Sov. Phys. JETP* **33** (4), 729–739.

D'IAKOV, S. P. 1958*b* Interaction of shock waves with small perturbations II. *Sov. Phys. JETP* **33** (4), 739–747.

FEDOROV, A. 2011 Transition and stability of high-speed boundary layers. *Annu. Rev. Fluid Mech.* **43**, 79–95.

JAMME, S., CAZALBOU, J. B., TORRES, F. & CHASSAING, P. 2002 Direct numerical simulation of the interaction between a shock wave and various types of isotropic turbulence. *Flow Turbul. Combust.* **68** (3), 227–268.

JIANG, G. S. & SHU, C. W. 1996 Efficient implementation of weighted ENO schemes. *Comput. Phys.* **126** (1), 202–228.

KERREBROCK, J. L. 1956 The interaction of flow discontinuities with small disturbances in a compressible fluid. PhD thesis, California Institute of Technology.

LARSSON, J., BERMEJO-MORENO, I. & LELE, S. K. 2013 Reynolds and Mach-number effects in canonical shock–turbulence interaction. *J. Fluid Mech.* **717**, 293–321.

LARSSON, J. & LELE, S. K. 2009 Direct numerical simulation of canonical shock/turbulence interaction. *Phys. Fluids* **21** (054102), 1–12.

LEE, S., LELE, S. K. & MOIN, P. 1993 Direct numerical simulation of isotropic turbulence interacting with a weak shock wave. *J. Fluid Mech.* **251**, 533–562.

LEE, S., LELE, S. K. & MOIN, P. 1997 Interaction of isotropic turbulence with shock waves: effect of shock strength. *J. Fluid Mech.* **340**, 225–247.

MA, Y. & ZHONG, X. L. 2003*a* Receptivity of a supersonic boundary layer over a flat plate. Part 1. Wave structures and interactions. *J. Fluid Mech.* **488**, 31–78.

MA, Y. & ZHONG, X. L. 2003*b* Receptivity of a supersonic boundary layer over a flat plate. Part 2. Receptivity to free-stream sound. *J. Fluid Mech.* **488**, 79–121.

MA, Y. & ZHONG, X. L. 2005 Receptivity of a supersonic boundary layer over a flat plate. Part 3. Effects of different types of free-stream disturbances. *J. Fluid Mech.* **532**, 63–109.

MCKENZIE, J. F. & WESTPHAL, K. O. 1968 Interaction of linear waves with oblique shock waves. *Phys. Fluids* **11** (11), 2350–2362.

MOORE, F. K. 1954 Unsteady oblique interaction of a shock wave with a plane disturbance. *NACA Tech. Rep. TR-1165*.

POTTER, J. L. & WHITFIELD, J. D. 1962 Effects of slight nose bluntness and roughness on boundary-layer transition in supersonic flows. *J. Fluid Mech.* **12** (4), 501–535.

RESHOTKO, E. 1976 Boundary-layer stability and transition. *Annu. Rev. Fluid Mech.* **8** (1), 311–349.

RIBNER, H. S. 1954 Convection of a pattern of vorticity through a shock wave. *NACA Tech. Rep. TR-1164*.

ROBINET, J. C. & CASALIS, G. 2001 Critical interaction of a shock wave with an acoustic wave. *Phys. Fluids* **13** (4), 1047–1059.

RYU, J. & LIVESCU, D. 2014 Turbulence structure behind the shock in canonical shock–vortical turbulence interaction. *J. Fluid Mech.* **756** (R1), 1–13.

SHU, C. W. & OSHER, S. 1988 Efficient implementation of essentially non-oscillatory shock-capturing schemes. *Comput. Phys.* **77** (2), 439–471.

STETSON, K. F., THOMPSON, E. R., DONALDSON, J. C. & SILER, L. G. 1984 Laminar boundary layer stability experiments on a cone at Mach 8. Part 2: Blunt cone. *AIAA Paper 1984-0006*.

SU, C. H. & GENG, J. L. 2017 Interaction of weak free-stream disturbance with an oblique shock: validation of the shock-capturing method. *Appl. Math. Mech. -Engl. Ed.* **38** (11), 1601–1612.

TIAN, Y., JABERI, F. A., LI, Z. & LIVESCU, D. 2017 Numerical study of variable density turbulence interaction with a normal shock wave. *J. Fluid Mech.* **829**, 551–588.

ZHONG, X. L. 1998 High-order finite-difference schemes for numerical simulation of hypersonic boundary-layer transition. *Comput. Phys.* **144** (2), 662–709.

ZHONG, X. L. & WANG, X. W. 2012 Direct numerical simulation on the receptivity, instability, and transition of hypersonic boundary layers. *Annu. Rev. Fluid Mech.* **44**, 527–561.